Visualizing a Convergence of Three Mitochondrial Molecule mRNAs for Drp1/Mfn2/Ucp4 on Soma of Cerebellar Purkinje Cells by RNAscope

Hui Liu
Fourth Military Medical University: Air Force Medical University
Tingting Luo
Fourth Military Medical University: Air Force Medical University
Feifei Wu
Fourth Military Medical University: Air Force Medical University
Baolin Guo
Fourth Military Medical University: Air Force Medical University
Kunlong Zhang
Fourth Military Medical University: Air Force Medical University
Shujiao Li
Fourth Military Medical University: Air Force Medical University
Xiaodong Li
Fourth Military Medical University: Air Force Medical University
Ruiqing Wang
Fourth Military Medical University: Air Force Medical University
Jinghao Chen
Fourth Military Medical University: Air Force Medical University
Lu Wang
Yan'an University
Yanling Yang
Fourth Military Medical University: Air Force Medical University
Ya-Yun Wang (wangyy@fmmu.edu.cn)
Air force Medical University https://orcid.org/0000-0003-3578-467X

Research Article

Keywords: Mitochondrial dynamic proteins, RNAscope, Purkinje cell, Cerebellum, Cre-LoxP mice

Posted Date: December 17th, 2021

DOI: https://doi.org/10.21203/rs.3.rs-1159900/v1

Abstract

We know little about how mitochondrial dynamics regulates in the Purkinje cells. To explore it, we first set up the Gad2-cre:ZsGreen-tdTomato$^{fl/fl}$ mice where Purkinje cells expressed tdTomato in the cerebellum. Secondly, double stainings verified tdTomato cells were Calbinin (CB)-positive Purkinje cells, but colocalized neither with astrocyte marker GFAP nor with microglia marker Iba1. Thirdly, application of RNAscope in situ hybridization with the identification of mRNAs of mitofusin 2 (*Mfn2*), calcium transporter (*Mcu* and *Nclx*) and uncoupling proteins (*Ucp2* and *Ucp4*) were used onto Purkinje cells for specific spatial analysis. Our findings demonstrated that *Mfn2* mRNAs expression was evident in Purkinje cells. And few expressions of *Ucp4* mRNAs were presented in dendritic shafts of Purkinje cells. It should be noted that *Mcu*, *Nclx*, and *Ucp2* mRNAs expression were only scattered on both soma and dendrites in Purkinje cells. The double RNAscope profiling of mitochondrial molecules showed *Mfn1* mRNAs are presented only in the soma of the Purkinje cells. Double RNAscope showed none of *Drp1* mRNAs were co-localized with *Mcu* mRNAs, as well as almost none of *Ucp2* mRNAs were co-localized with *Mfn2* mRNAs. All of these results showed the mitochondrial *Drp1*/ *Mfn2*/ *Ucp4* convergence on the Purkinje cells. Finally, present research focuses on developing new and more specific molecules tuning the activity of the Purkinje cells activate or inactivate and opening therapeutic windows for Purkinje cells-related diseases. The molecular identification of potential drug targets, mechanism of action, and structural basis of their activity will crucially enable preclinical development.

Highlights

1. We firstly constructed the Cre-LoxP mice with beautiful cerebellar Purkinje cells expressing tdTomato fluorescence.
2. By using RNAscope in situ hybridization, we found a convergence of mRNAs for three mitochondrial molecules, *Drp1*/ *Mfn2*/ *Ucp4*, on the Purkinje cells.
3. Surprisingly, two mitochondrial calcium buffering proteins of *Mcu* and *Nclx*, another fusion protein *Mfn1*, as well as another mitochondrial uncoupling protein *Ucp2* could not be found abundantly in the Purkinje cells.
4. All of these results showed the mitochondrial *Drp1*/ *Mfn2*/ *Ucp4* convergence on the Purkinje cells and provided insights into the pathogenic mechanism underlying cerebellum-related neurological diseases.

Introduction

Cerebellum has been one of novel target for the treatment towards movement disorder. Cerebellar cortex contains three layers, includes molecular layer (basket cells, stellate cells), Purkinje layer (Purkinje cells,) and granular layer (granular cells, Golgi cells) [1]**.** Purkinje cells are the sole output of the computational circuitry of the cerebellar cortex and provide the signals required for motor planning, execution and coordination in their rate of firing and pattern of activity [2]. Malfunction of these neurons often results in

cerebellar ataxia: a disorder characterized by poor balance, loss of posture and difficulties in performing rapid coordinated movements [3,4]. Purkinje cells fire spontaneously with highly regular pacemaking and their neurotransmission depends on more than 150,000 excitatory and inhibitory synapses [4]. So Purkinje cells have a particular dependence on precise control of mitochondrial dynamics.

Mitochondria are dynamic double-membrane-bound organelles that are associated with ATP generation, calcium regulation, and the biosynthesis of aminoacids, lipids, and nucleotides [5]. In the past few years , progress in the field of mitochondrial biology has shown that mitochondrial activities have important implications for the cerebellum [6]. Mitochondrial fusion and fission, calcium buffering handling, and uncoupling process are crucial for functional maintenance of Purkinje cells [7]. Understanding these mechanisms will enable discovery and development of new strategies for Purkinje cell related treatment.

Although there is a clearly emerging link between mitochondrial defects and Purkinje cells, its molecular basis is poorly understood. Which mitochondrial fusion and fission proteins affect the mitochondria of Purkinje cells, and how about mitochondrial calcium buffering proteins and uncoupling proteins? To examine the distribution pattern of mitochondrial molecules in purkinje cells, we used Cre-LoxP system to generate a conditional knock-in mice with specific fluorescence in GABAergic purkinje cell. In the Gad2-ires-Cre mice, all of GABAergic neurons contained Cre recombinase. In ZsGreen-tdTomato$^{fl/fl}$ mice, the green fluorescent protein ZsGreen and the red fluorescent protein tdTomato were knocked into the mice and the loxP sites were buried on both sides of ZsGreen. After crossing of these two mice, the Purkinje cells could be easily identified as red fluorescent protein under confocal microscopy. These mice were then used for the following immunofluorescence and hybridization.

By using RNAscope in situ hybridization, we found a convergence of mRNAs for three mitochondrial molecules, *Drp1*/ *Mfn2*/ *Ucp4*, on the Purkinje cells. Surprisingly, two mitochondrial calcium buffering proteins of *Mcu* and *Nclx*, another fusion protein *Mfn1*, as well as another mitochondrial uncoupling protein *Ucp2* could not be found abundantly in the Purkinje cells. Our results indicated that the *Drp1*/ *Mfn2*-dependent fission and fusion on mitochondrial outer membrane, as well as *Ucp4*-dependent ROS regulation on mitochondrial inner membrane are a fundamental, targetable determinant of Purkinje cell. Our work provided a framework for understanding mitochondrial plasticity at Purkinje cell level, and could suggest ways of modulating mitochondrial activity to treat cerebellum-related diseases. In addition, we think that visualization of gene expression with Purkinje cells-specific spatial context can be achieved by combining the highly sensitive and specific RNAscope in situ hybridization with Gad2-cre:ZsGreen-tdTomato$^{fl/fl}$ mice.

Materials And Methods

2.1 Animals and mouse breeding

To examine the distribution pattern of mitochondrial molecules in purkinje cells, we used cre-*loxP* system to generate a conditional knock-in mice with specific fluorescence in GABAergic purkinje cell.

2.1.1 Gad2-ires-Cre mice

The C57BL/6-Gad2$^{EM1(IRES-ICRE-PA)SMOC}$ (named as Gad2-ires-Cre) mice were purchased from Institute of Model Zoology, Nanjing University with the Product Number of D000668, previously reported [8]. It is well-known that GABA (g-aminobutyric acid) in mammals was synthesized by two glutamic acid decarboxylases (GAD) GAD67 and GAD65 [9]. These two proteins were encoded by Gad1 and Gad2 genes. The Gad2-ires-Cre mice inserted an internal ribosome entry site (ires) and a Cre recombinase sequence at the 3' end of the Gad2 allele, so that all of GABAergic neurons contained Cre recombinase.

2.1.2 LoxP-flanked (floxed) ZsGreen-tdTomato mice

The *loxP*-flanked (floxed) ZsGreen-tdTomato mice used here are *B6/JGpt-H11*$^{em1Cin(CAG-LoxP-ZsGreen-Stop-LoxP-tdTomato)/Gpt}$ mice (ZsGreen-tdTomato$^{fl/fl}$), which were purchased from Jiangsu Jicui Yaokang Biological Technology Co. Ltd with the Product Number of E2101190037, reported previously [10]. In ZsGreen-tdTomato$^{fl/f}$ mice, the green fluorescent protein ZsGreen and the red fluorescent protein tdTomato were knocked into the mice H11 gene site and the *loxP* sites were buried on both sides of ZsGreen. Zsgreen is expressed in all cells (including the GABAergic neurons) of the ZsGreen-tdTomato$^{fl/fl}$ mice with no special promoter [10].

2.1.3 Crossing the two mice

In order to distinguish the GABAergic neurons from other cells, we across the two mice mentioned above. After crossing of these two mice, Cre recombinase will cut the loxP sites, and green fluorescent protein ZsGreen will be cut out. Considering only GABAergic neurons contained Cre recombinase, therefore, only GABAergic neurons in the newly generated transgenic (Gad2-cre:ZsGreen-tdTomato$^{fl/fl}$) mice would transfer from expressing green fluorescence to expressing tdTomato fluorescence protein. It should be emphasized that GABAergic neurons in cerebellum also include basket cells or Golgi cells, but Purkinje cells have the particularity which PC are arranged in neat rows, which could be distinguished obviously for the further observation. Therefore, Purkinje cells of (Gad2-cre:ZsGreen-tdTomato$^{fl/fl}$) mice could be easily identified under confocal microscopy. These mice were then used for the following immunofluorescence labeling and single RNAscope in situ hybridization.

It should be indicated that the normal adult C57BL/6 mice were used for double RNAscope in situ hybridizations.

All of the mice are kept in a barrier facility, and all animal experiments were conducted in accordance with the procedures approved by the Ethical Committee of the Air Force Medical University and followed the institutional guidelines for the use of laboratory animals.

Animals were housed at a constant 23 °C in a 12 h light/dark cycle (lights off at 20:00), with food and water available. The day of birth was considered as postnatal day 0 (P0).

2.2 Genotyping

Genotype was identified by PCR with genomic DNA obtained from the tails. The primers sequences and PCR programs were listed in **Table 1.**

2.3 Immunofluorescence labeling

To verify the reliability of red tdTomato fluorescence within Purkinje cell in the generated Gad2-cre:ZsGreen-tdTomato$^{fl/fl}$ mice, immunofluorescence labeling was conducted according to the methods described previously with minor modifications [11].

Six eight-week male Gad2-cre:ZsGreen-tdTomato$^{fl/fl}$ mice were perfused transcardially with 0.1 M phosphate buffer (PB; pH 7.4) followed by 4% paraformaldehyde in 0.1 M PB. The whole cerebellum were obtained and postfixed with the same fixative for 4 h, placed in 30% (w/v) sucrose reliability solution in 0.05 M PB solution (PBS; pH 7.4) overnight at 4 °C, and cut into sagittally 30 mm thick sections on a freezing microtome. Then the cerebellum sections were mounted onto the slides and incubated in 0.01 M PBS supplemented with 3% hydrogen peroxide for 10 min to block endogenous peroxidase and then in a blocking buffer containing 5% BSA/10% normal goat serum/0.25% Triton X-100 for 60 min at room temperature to prevent nonspecific staining. Following this, the sections were incubated in the blocking buffer for 60 min at room temperature and then in a solution containing primary antibodies of the marker of Purkinje cells (Calbindin, CB), the marker of granular cells (NeuN), the marker of astrocytes (GFAP), the marker of microglia (Iba1) **(Table 2)** from different species simultaneously for 18 h at 4 °C. After washing, sections were incubated with appropriate secondary antibodies **(Table 2)** for 2 h at room temperature.

It should be indicated that in the cerebellum of Gad2-cre:ZsGreen-tdTomato$^{fl/fl}$ mice, Purkinje cells expressed bright tdTomato fluorescence, while non-GABAergic expressed bright ZsGreen fluorescence. So we observed the sections under a confocal laser scanning microscope (FV-1000, Olympus, Tokyo, Japan) with a confocal depth of 1.0 mm. The mode of triple immunofluorescence labelings was used. The laser beams and filters for ZsGreen were the 488 nm of excitation and 525 nm of emission, the parameters for tdTomato were 550 nm of excitation and 570 nm of emission, and for the antibody stained were 649 nm of excitation and 670 nm of emission. Around 30 slices obtained from 6 mice (5 slices per mouse) were randomly chosen. Images were carried out by individuals blinded towards the experimental groups.

2.4 Imaris file format description of immunofluorescence labeling

In order to more accurately imagine three-dimensional (3D) structure of GABAergic Purkinje cells expressing red fluorescence in the cerebellum of Gad2-cre:ZsGreen-tdTomato$^{fl/fl}$ mice, Imaris × 64 image analysis software (version 9.6.0, Oxford Instruments, England) was used. The Imaris file had high performance rendering and processing of laser confocal images. The Path Attribute Description was /DataSet/ResolutionLevel 0/TimePoint 0/Channel 0 with information concerning resolution 0, time point 0 and channel 0. ImageSizeX = 285, indicating the size in X in pixel for Resolution Level 0; ImageSizeY = 218, indicating the size in Y in pixel; ImageSizeZ = 64, indicating the size in Z in pixe.

2.5 Single and double RNAscope in situ hybridization

To provide Purkinje cells-specific spatial analysis about the RNAs profiling of important mitochondrial molecules, the single RNAscope technology was conducted on the cerebellum sections from the Gad2-cre:ZsGreen-tdTomato$^{fl/fl}$ mice. Moreover, in order to verify the characterization of the molecules [12], we conducted double RNAscope assays to simultaneously detect two targets on the normal mice section. In our research, 3 mice were counted into our study, and each mouse was photographed with 3 images.

2.5.1 Probes

The probes used in RNAscope were divided into two types: first for molecules on outer mitochondrial membrane (OMM) including *Drp1* (mitochondrial fission protein), *Mfn1* and *Mfn2* (mitochondrial fusion protein); second for molecules on the inner mitochondrial membrane (IMM) including *Mcu* (mitochondrial calcium intruder), *Nclx* (mitochondrial calcium intruder), *Ucp2* and *Ucp4* (mitochondrial uncoupling protein); the negative (dapB) and positive (Polr2a/PPIB/UBC) controls; whose information was provided in **Table 3**.

2.5.2 Tissue preparation

RNAscope® Multiplex Fluorescent Reagent Kit manual was performed as instructed by Advanced Cell Diagnostics (ACD). Newly prepared 1× phosphate buffered saline (PBS, pH 7.4) and 4% paraformaldehyde (PFA, pH 7.4) were used to perfuse the heart of mice. Tissues of interest were then removed in 4% PFA at 4˚C for 24 hours, and then treated with sucrose solutions for dehydration. The tissues were cryostat-sectioned at 15μm onto SuperFrost Plus charged slides. Sections were only briefly thawed to adhere to the slide but were immediately returned to the -20˚C cryostat chamber until completion of sectioning. Before used for following histology, the slides were baked in a chamber at 37˚C for 3 hours. Slides were removed from the baking chamber and immediately transferred to 1× PBS at room temperature for 5 minutes. Each slide was incubated with Hydrogen peroxide at room temperature for 10 minutes. After being washed by distilled water, the slides were treated by the boiled target retrieval solutions at 96˚C for 10 minutes. The tissues were placed in distilled water immediately at room temperature, and then dehydrated in 100% ethanol for 3 minutes. The slides were air-dried briefly and then boundaries were drawn around each section using a hydrophobic pen (CIRISC PAP pen, I.S. CIRCLE WRITER, Japan). When hydrophobic boundaries had dried, protease III reagent was added to each section until fully covered, incubation at 40˚C for 30 minutes. During this period, slides were placed in a prewarmed humidity control tray containing dampened filter paper in the HybEZ oven (ACD).

2.5.3 Hybridization

Only one probe or a mixture of two probes were then added to each slide. Channel 1, Channel 2, and Channel 3 probes (50: 1: 1 dilution, as directed by ACD due to stock concentrations), which were pipetted onto each section until fully submerged. This was performed on one slide at a time to avoid liquid evaporation and section drying. The humidity control tray was placed in a HybEZ oven (ACD) for 2

hours at 40˚C. A table of all the probes used is shown in **Table 3**. After probe incubation, the slides were washed twice in 1× RNAscope® wash buffer and returned to the oven for 30 minutes after submersion in AMP-1 reagent. Washes and amplification were repeated using AMP-2, and AMP-3 reagents with a 30-, and 15-minute incubation period, respectively. HRP-C1 signal, HRP-C2 signal, and HRP-C3 signal were developed respectively. Different dyes were needed to differentiate probes derived from three kinds of channels. We employed Opal 520 (FP1487001KT, PerkinElmer) to mark channel 1 probes, Opal 570 (FP1488001KT, PerkinElmer) to mark channel 2 probes, and Opal 690 (FP1497001KT, PerkinElmer) to mark channel 3 probes. Slides were incubated with DAPI for 5 minutes before being washed, air-dried, and coverslipped with Prolong Gold Antifade mounting medium.

2.6 RNAscope images acquisition and semi-quantitative analysis

Anatomical structures were analyzed in sagittal sections and mapped according to Paxinos and Franklin atlas [13] and Allen map (http://mouse.brain-map.org/static/atlas)**.** Fluorescent signals of mRNA hybridization for mitochondrial molecules were imaged with a 10×, 20×, 40× and 60× objective lens on a a confocal laser scanning microscope (FV-1000, Olympus, Tokyo, Japan). All microscope and camera settings were identical for all images. We used the ImageJ64 software (National Institute of Health. Bethesda, MD, USA), as previously described [14].

The RNAscope assay used a semi-quantitative H scoring guideline to evaluate the staining results. We scored the number of dots per Purkinje cell rather than the signal intensity to interpret RNAscope staining, because the number of dots correlates to the number of RNA copy numbers, whereas dot intensity reflects the number of probe pairs bound to each molecule [15]. In the present study, H score was to visualize the dynamic expression level by binning the percentage of cells with a certain expression level or number of dots in one bin. The number of bins ranges from 0 - 4 according to the ACD scoring system. The overall H score can range from 0 - 400 and is calculated as shown:

$$\text{H-score} = \sum_{Bin\ 0\rightarrow 4} (\text{ACD score or bin number x percentage of cells per bin})$$

Negative control (dapB) stained slides were always imaged at the settings used for target probe imaging and did not result in appreciable signal. Positive control (Polr2a/PPIB/UBC) should be indicated as successful staining which have a score ≥2.

Purkinje cells brought into study were a string of cells that are neatly arranged with a typical appearance, range in width from 10.31 μm to 16.92 μm and in height from 8.7 μm to 19.65 μm. Moreover, the selected cells had droplet soma and cypress-shape dendrites. We had to admit that there must be some basket cells have been included in the statistical analysis, but there were no methods to completely exclude them for us. What's more, given the small proportion of basket cells in the Purkinje cells layer reported by Fagan M et al. [16,17], we did not believe that it would cause our results far from the fact.

2.7 Statistical analysis

Figures for RNAscope and Immunofluorescence labeling are representative of sections obtained from three animals. Data for Figure 4, expressed as the mean ± SEM (sections obtained from five animals), were analyzed using one-way analysis of variance (ANOVA) with Bonferroni's multiple comparison post hoc test using GraphPad Prism software v.5.0 (Graphpad). A *p*-value < 0.05 was considered statistically significant.

Results

3.1 Characteristic of tdTomato cells in GAD2-cre;ZsGreen-tdTomatofl/fl mice

Firstly, we used a Cre-*loxP* strategy to generate conditional knock-in mice with specific fluorescence in GABAergic Purkinje cell **(Fig. 1A)**. The Gad2-ires-Cre mice were inserted a Cre recombinase sequence at Gad2 allele to make all GABAergic neurons containing Cre recombinase.

So in the ZsGreen-tdTomato$^{fl/f}$ mice, ZsGreen and tdTomato were knocked in and the *loxP* sites were buried on both sides of ZsGreen. After crossing these two mice, all GABAergic neurons would transfer from expressing ZsGreen to expressing tdTomato due to Cre recombinase cutting loxP sites. The genotyping strategy used four sets of primers to produce four bands of 1465 bp (for ZsGreen-tdTomato with loxP site), 285 bp (for wild type site), 352 bp (for Cre recombinase), and 250 bp (for wild type site) **(Fig. 1B)**.

Secondly, average body appearances were compared between control Gad2-cre mice and the Gad2-cre:ZsGreen-tdTomato$^{fl/fl}$ mice **(Fig. 1C)**. Interestingly and apparently, Gad2-cre:ZsGreen-tdTomato$^{fl/fl}$ mice showed dazzling green light visible to the naked eye in external auricle skin (arrow), plantar skin (arrow), as well as perianal skin (arrow), although the body weights of both types of mice had no significant difference. Moreover, the brains of Gad2-cre:ZsGreen-tdTomato$^{fl/fl}$ mice showed green fluorescence, while the brains of control Gad2-cre mice showed normal pink, which made it very easy to distinguish the GABAergic knock-in mice.

Thirdly, the confocal microscope images were taken to show that Purkinje cells expressed tdTomato in the cerebellum of Gad2-cre:ZsGreen-tdTomato$^{fl/fl}$ mice, while non-GABAergic cells expressed ZsGreen **(Figs. 1D and 1E)**. We could find that the neuronal bodies of Purkinje cells with red fluorescence (asterisk marked in **Fig. 1E**) were aligned like dominos stacked throughout the PCL (purkinje cell layer), also they had large dendritic arbors (**Fig. 1E**) like within the molecular layer (ML) and sent axons like bright flame out off cerebellar cortex (**Fig. 1E**), therefore they left for the dark area of granular layer (GCL) which were occupied by green non-GABAergic cells (**Fig. 1E**). It should be emphasized that GABAergic neurons in the cerebellum also include basket cells or Golgi cells, but Purkinje cells have the particularity that PC are arranged in neat rows and colocalized with CB (**Fig. 2A**), which could be distinguished obviously for further observation. Therefore, Purkinje cells of (Gad2-cre:ZsGreen-tdTomato$^{fl/fl}$) mice could be easily identified under confocal microscopy.

Fourthly, the Imaris file was designed to allow better visualization of Purkinje cells specifically expressed tdTomato fluorescence in GAD2-cre:ZsGreen-tdTomato$^{fl/fl}$ mice **(shown in Videos. 1-3)**. We could see that the neuronal bodies of Purkinje cells with red fluorescence were aligned like dominos stacked throughout the PCL, while the dark area of granular layer (GCL) were occupied by green non-GABAergic cells.

3.2 Double stainings verified tdTomato cells were Purkinje cells

Previous studies have shown that Cerebellar Purkinje cells could be marked by Calbinin (CB) [18], while the granular cells were marked by NeuN [19]. In addition, the astrocytes (as GFAP as marker) and microglia (as Iba1 as marker) were believed to be scattered throughout the cerebellar cortex [20,21]. So, in order to verify the cells expressing tdTomato fluorescence in cerebellum of Gad2-cre:ZsGreen-tdTomato$^{fl/fl}$ mice were exclusively Purkinje cells, the present immunostainings with the four antibodies mentioned above were observed under the psudo blue color. The percentage of blue cells in the distinct cell subgroups was determined.

To figure out if tdTomato-positive cells represented the Purkinje cells, we calculated the fluorescence area displayed by various cell markers. In Figure 2A, the total fluorescent area of tdTomato was 709268 μm^2, of which 667366 μm^2 was co-marked with CB, accounting for 94%. It could be indicated that dominos stacked - like tdTomato-positive cells (red) were 95.0% colocalized with CB (green) **(Fig. 2A)**, so that they appeared the color of purple. On the contrary, the total fluorescent area of tdTomato is 567296 μm^2, of which only 26572 μm^2 was co-marked with NeuN, accounting for 5%. Immunostaing data showed few of tdTomato-positive cells were colocalized with NeuN, the marker of granular cells **(Fig. 2B)**. Moreover, the total fluorescent area of tdTomato was 560832 μm^2 and there was no contact between tdTomato and GFAP. It was same to GFAP that Ibal1 was far from tdTomato (covered 531440 μm^2). Almost none of tdTomato-positive cells were colocalized either with astrocyte marker GFAP **(Fig. 2C)** or with microglia marker Iba1 **(Fig. 2D)**.

We have noticed that there was 5% of NeuN+ tdTomato+ cells shown in panel B. We should say that these structures are located in the layer of granular cell. While in the present study, what we have calculated and analyzed have focused on the Purkinje cell dendrites in the molecular layer and their soma in the layer of Purkinje cells. So we think the 5% of NeuN+ tdTomato+ cells will not disturb our results so far.

At the same time, ZsGreen-positive cells were densely distributed cross GCL, scattered though PCL, and few in ML **(Fig. 2)**. The total fluorescence area of ZsGreen was 31468 μm^2, of which 1% was co-marked with CB and covered 249 μm^2. Double stainings showed almost none of these green cells were colocalized with Purkinje cell marker CB **(Fig. 2A)**. On the contrary, the total fluorescence area of ZsGreen was 635684 μm^2, of which 95% was co-marked with NeuN and covered 577536 μm^2. These green cells mainly consisted of NeuN-positive granular cells **(Fig. 2B)**. The total fluorescence area of ZsGreen was 662256 μm^2, of which 5% was co-marked with GFAP and covered 32704 μm^2. And the total fluorescence

area of ZsGreen was 694960 μm^2, of which only 1% was co-marked with Iba1 and covered 8042 μm^2. Our results also confirmed that ZsGreen-positive cells were not astrocyte **(Fig. 2C)** or microglia **(Fig. 2D)**.

These data suggested that tdTomato-positive cells were primarily expressed in GABAergic Purkinje cells within cerebellar cortex. Then, RNAscope in situ hybridization was performed to examine the presence of seven mitochondrial proteins within the Purkinje cells of Gad2-cre:ZsGreen-tdTomato$^{fl/fl}$ mice.

3.3 Application of RNAscope in situ hybridization onto GAD2-cre:ZsGreen-tdTomato$^{fl/fl}$ mice for Purkinje cell - specific spatial analysis

Identification of mRNAs of mitochondrial fusion (*Mfn2*), calcium transporter (*Mcu* and *Nclx*) and uncoupling proteins (*Ucp2* and *Ucp4*) in Purkinje cells in the cerebellar cortex of GAD2-cre:ZsGreen-tdTomato$^{fl/fl}$ mice with RNAscope probes. The red cells were Purkinje cells; green cells were non-GABAergic cells; blue dots were RNA fluorescence. Moreover, ACD scoring system was used to calculate the overall H scores of Dendritic Weighted Formula (DWF) and Soma Weighted Formula (SWF).

Guan, J et al. and Berrebi, A et al. reported that *Pcp2* has the potent to sketch the boundary of PC well and is primarily regarded as a well-chosen marker of PC. And because of the existing conditions of our group, *Pcp2* was chosen into our research to represented the Purkinje cells [22,23]. In our study, the confocal images were photographed under laminar scanning, which means the tissue was scanned in layers along the Z-axis. The figure 2A presented in this article was one of the 5-layer scanning images, so it seems that some segments were positive for CB or tdToamto alone. In order to prove that tdTomato-positive cells were indeed Purkinje cells and co-labeled with CB, we combined the 5 layers and used the Section module in Imaris software, which can enlarge the local area for us to observe the co-localization of cells **(See in supplementary Fig. 1)**. In the Section module, we cropped the part of image of interest along X-axis and Y-axis, XB represents for the image of X direction and YC for the Y direction. we selected two regions from the supplementary figure 2A that appeared to be co-labeled by CB and tdToamto showed in **Figure 2A and 2B**, and it was no effort to see CB and tdTomato co-labeled from their respective X and Y axis. Then we chose two areas where cells were positive for tdToamto alone under the naked eye, and to our surprise we observed CB and tdTomato co-labeled **(Supplementary Fig. 2C and D)**. We also captured the part of Figure A in which only CB appeared to be obvious, and unsurprisingly, we saw the same co-labeling phenomenon **(Supplementary Fig. 2E)**. To further illustrate, the Section module displayed adjacent colors only if they are co-localization. We picked two parts of granular layer in Figure A that completely presented CB **(Supplementary Fig. 2F and G)** or tdToamto **(Supplementary Fig. 2H and I)** alone, and it turned out that there was no tdToamto or CB respectively.

3.3.1 *Mfn2* mRNA

Mitofusin 2 (*Mfn2*) controls the fusion of the outer mitochondrial membrane (OMM), but the physiological function of *Mfn2* in Purkinje cells remains unclear. Our data firstly demonstrated that *Mfn2* mRNAs expression was evident in Purkinje cells in the cerebellum of Gad2-cre:ZsGreen-

tdTomato$^{fl/fl}$ mice **(Fig. 3A)**. Moreover, 76.5% dendrite shafts were ranked as Bin 1 because they only had 1-3 dots per shaft **(Fig. 3B)**; On the contrary, 71.8% soma were ranked as Bin 4 because they had more than 15 dots per cell body **(Fig. 3C)**. The overall H scores of DWF and SWF were calculated as 60 and 139, respectively **(Table 4)**.

3.3.2 *Mcu* mRNA

Mitochondrial Ca^{2+} uptake is mediated by the Mitochondrial Calcium Uniporter (*Mcu*) complex, located on the inner mitochondrial membrane (IMM). Our data confirmed the previous report [7] that few *Mcu* mRNAs expressions were present on Purkinje cells in cerebellum of Gad2-cre:ZsGreen-tdTomato$^{fl/fl}$ mice **(Fig. 3D)**. Moreover, 57.1% dendrite shafts were ranked as Bin 0 because they had no dot per shaft **(Fig. 3E)**; Similarly, 58.1% soma were also ranked as Bin 1 **(Fig. 3F)**. The overall H scores of DWF and SWF were high as 70 and 22, respectively **(Table 4)**.

3.3.3 *Nclx* mRNA

Conversely to *Mcu*, Ca^{2+} release is under the control of the Na^{+}/Ca^{2+} exchanger, encoded by the *Nclx* gene, located on IMM. Our data firstly demonstrated that *Nclx* mRNAs expression were only scattered on both soma and dendrites in Purkinje cells in cerebellum of Gad2-cre:ZsGreen-tdTomato$^{fl/fl}$ mice **(Fig. 3G)**. About 91.7% dendrite shafts were ranked as Bin 0 because they had no dot per shaft **(Fig. 3H)**; Similarly, 58.3% soma were ranked as Bin 1 because they had only no more than 3 dots per cell body **(Fig. 3I)**. The overall H scores of DWF and SWF were 4 and 31, respectively **(Table 4)**.

3.3.4 *Ucp2* mRNA

Ucp2 are IMM proteins that may regulate mitochondrial energy metabolism and ROS generation. Our data firstly demonstrated that unexpectedly, few *Ucp2* mRNAs expressions were presented in Purkinje cells in cerebellum of Gad2-cre:ZsGreen-tdTomato$^{fl/fl}$ mice **(Fig. 3J)**. Moreover, 75.0% dendrite shafts and 41.2% soma were ranked as Bin 0 because they had no dot **(Figs. 3K and 3L)**. The overall H scores of DWF and SWF were only 15 and 27, respectively **(Table 4)**.

3.3.5 *Ucp4* mRNA

Ucp4, another IMM protein for regulating mitochondrial energy metabolism and ROS generation, has been looked like a twin of *Ucp2*. Our data confirmed that few *Ucp4* mRNAs expressions were presented in dendritic shafts of Purkinje cells in cerebellum of Gad2-cre:ZsGreen-tdTomato$^{fl/fl}$ mice **(Fig. 3M)**. However, 67.6% soma were ranked as Bin 3 because they had 10-15 dots per cell body **(Figs. 3N and 3O)**. The overall H scores of DWF and SWF were only 14 and 103, respectively, suggesting the high expression in the soma of PC and low in the dendrites **(Table 4)**.

3.4 Double RNAscope profiling of mitochondrial molecules in cerebellar cortex of normal mice

In order to verify the characteristics of the molecules, we conducted double RNAscope assays to simultaneously detect two targets on the normal mice section.

3.4.1 *Mfn1* (green) and *Pcp2* (red)

For the reason that *Pcp2* has the potent to sketch the boundary of PC well and is primarily regarded as a well-chosen marker of PC, *Pcp2* was chosen into our research to represented the Purkinje cells. Because our present *Mfn1* probe was not suitable for the detection in the samples from GAD2-cre;ZsGreen-tdTomato$^{fl/fl}$ mice, we did double RNAscope profiling of *Mfn1* mRNA (green) in Purkinje cells (red) which were distinguished by the red fluorescence with the mRNA probe of Purkinje cell protein-2 (*Pcp2*) gene **(Fig. 4A)**. Higher magnification images showed that within the PCL, some dots could be found in the soma of Purkinje cells (red) **(Fig. 4B)**. However, within both the ML and the GCL, few green dots could be found in the dendrites or axons of Purkinje cells, respectively **(Fig. 4B)**. ACD quantification confirmed the middle-level expression level of *Mfn1* mRNAS in soma **(Fig. 4C)**. The calculation of the percent of double *Pcp2-Mfn1* stainings on single *Pcp2*-positive expressions confirmed the very low colocalization both in the ML and in the GCL **(Fig. 4D)**. The data suggested *Mfn1* mRNAs are present only in the soma of the Purkinje cells, instead of processes.

3.4.2 *Drp1* (green) and *Mcu* (red)

According to our previous report [24], we demonstrated that *Drp1* was overexpressed in the cerebellum Purkinje layer, while *Drp1* and GAD67 also colabeled well in this area. *Drp1* and GAD67 colabeling was lower in other nuclei. As discussed in methods, GABA in mammals was synthesized by GAD67 and GAD65, thus, GABAergic neurons in the cerebellum Purkinje layer (Purkinje cells) are specifically labeled with GAD67-GFP fluorescence in our previous report, which indicated that *Drp1* can mark Purkinje cells based on its localization in the Purkinje cell layer. Therefore, based on the opinion that Purkinje cells could be distinguished by *Drp1* fluorescence. Because our previous report had presented the detailed distribution of *Drp1* mRNA in the cerebellar cortex of normal mice by in situ hybridization method, the present double RNAscope profiling was to verify the distribution of *Mcu* in Purkinje cells because these cells could be distinguished by *Drp1* fluorescence **(Fig. 5A)**. Higher magnification images confirmed that green *Drp1*-positive dots could outline the soma of Purkinje cells **(Fig. 5B)**. Our results of Gad2-cre:ZsGreen-tdTomato$^{fl/fl}$ mice by in situ hybridization had showed that a number of dots of *Mcu* mRNAs were present in processes and soma of Purkinje cells **(Fig. 3D)**. Here, the double RNAscope profiling was consistent with the previous distribution pattern. Unexpectedly and interestingly, almost none of dots of *Drp1* mRNAs were co-localized with dots of *Mcu* mRNAs, wherever at ML, PCL or GCL **(Fig. 5C).** The data suggested the separation of *Drp1* on OMM and *Mcu* on IMM even though they were all abundant in the Purkinje cells.

3.4.3 *Ucp2* (green) and *Mfn2* (red)

Our results of Gad2-cre:ZsGreen-tdTomato$^{fl/fl}$ mice by RNAscope in situ hybridization had showed that a number of dots of *Mfn2* mRNAs were present in soma of Prukinje cells, although this kind of high level

did not happen in dendrites of Purkinje cells **(Figs. 3A-3C)**. On the contrary, the dots of *Ucp2* mRNAs were scattered not only on the soma but also on the dendrites of Purkinje cells **(Figs. 3J-3L)**. The present double RNAscope profiling confirmed the dense expressions of *Mfn2* in soma of the Purkinje cells **(Fig. 6A),** so that in the higher magnification images these cells could be distinguished by *Mfn2* red fluorescence **(Fig. 6B)**. Moreover, unsurprisingly, almost none of dots of *Ucp2* mRNAs were co-localized with dots of *Mfn2* mRNAs **(Fig. 6C)**. The data verified the presence of *Mfn2* but the nonexistence of *Ucp2* on the Purkinje cells.

Discussion

To explore the mitochondrial mechanisms of Purkinje cells, we first set up a transgenic mice in which Purkinje cells could be distinguished easily by expressing red fluorescence. We then detected spatial RNA profiling of seven mitochondrial molecules, including dynamin-related protein-1 (*Drp1*), mitochondrial calcium uniporter (*Mcu*); mitofusion 1 and 2 (*Mfn1*/2), sodium/lithium/calcium exchanger (*Nclx*), and uncoupling protein 2 and 4 (Ucp2/4), by RNAscope combined with ACD quantification. We finally proposed a mitochondrial *Drp1*/*Mfn2*/*Ucp4* convergence on the Purkinje cells, which would make up a mitochondrial quality control system. Our results establish a framework for understanding the pathogenic mechanism underlying cerebellum-related neurological diseases.

4.1 *Drp1*/*Mfn1*/*Mfn2*

Mitochondrial fission and fusion play critical roles in creating new mitochondria and removing damaged mitochondria. In mammalian cells, fission/fusion events are mainly mediated by several large dynamin-related GTPase proteins, including conserved dynamin-related GTPase (*Drp1*), conserved dynamin-related GTPase mitofusion 1 and 2 (*Mfn1* and 2), and optic dominant atrophy 1 (Opa1). Our lab have published the data previously about the expression of *Drp1* at high level on the soma of cerebellum Purkinje cells by the combination of immunohistochemistry and in situ hybridization on GAD67 (glutamic acid decarboxylase 67) - GFP (green fluorescent protein) transgenic mice [24]. The present findings have confirmed the distribution pattern of *Drp1* on Purkinje cells. These data suggest that the mitochondrial fission in Purkinje cells may be dependent on the mitochondrial fission mediator, *Drp1*. In fact, mitochondrial fission mediated by the GTPase *Drp1* is an attractive drug target in neurodegenerative disorders [25, 26]. Basal *Drp1*-dependent mitochondrial fission is required for mitochondrial trafficking to synapses, mitochondrial quality control, and brain development [27-29]. *Drp1* is highly conserved and contains many critical functional features that correspond to specific target structures within the enzyme, such as GTP binding, GTP hydrolysis, self-assembly and protein interactions with key functions in mitochondrial division [30, 31]. While the fission defects may limit mitochondrial motility, decrease energy production, promote oxidative stress and lead to accumulating of mtDNA defects, thereby promoting neuronal dysfunction and cell death [32, 33]. Thus, regardless of the different upstream stress stimulus, *Drp1*-mediated mitochondrial fragmentation and downstream mitochondrial pathways play a major role for the fate of Purkinje cells. Significantly, *Drp1* must be an efficient strategy for the neuroprotection against multiple cerebellar damage.

The finding of dense distribution of *Mfn2* on Purkinje cells deserves high attention for four reasons. First, the mutations in *Mfn2* have been found to cause a human neurodegeneration disease, Charcot-Marie-Tooth neuropathy type 2A [34-37]. Second, our data have supported previous paradigm that *Mfn2* is expressed at significantly greater levels in Purkinje cells than is *Mfn1* [34]. Third, it has been reported that Purkinje cells require *Mfn2* but not *Mfn1* for cell survival and dendritic outgrowth [34-36]. Fourth, *Mfn2*-deficient Purkinje cells have shown impaired respiratory complex activity and defects in inner membrane structure characteristic of respiratory dysfunction [34]. Our RNAscope studies provide insight into the dependence of the fusion of outer mitochondrial membrane (OMM) of soma of Purkinje cells on the molecular *Mfn2*.

In fact, neurodegeneration in neurodegenerative diseases has been related to several mitochondrial dynamics imbalances such as excessive fragmentation of mitochondria, impaired mitophagy, and blocked mitochondrial transport in axons. Our findings raise the intriguing possibility that a convergent pathway underlies the pathogenesis of neurodegenerative disorders. Nonetheless, the exact role of *Drp1*/*Mfn2*-dependent mitochondrial dynamics in Purkinje cells requires further investigation.

4.2 *Mcu* and *Nclx*

Mitochondrial Ca^{2+} homeostasis plays a central role in nervous system. Previous studies have suggested that dysfunction of calcium homeostasis is associated with oxidative stress and many neurological diseases [38-46]. In Purkinje cells, Bonnan A et al. have found that the dendritic Ca^{2+} transients are sufficient, potent triggers of plasticity induction that instruct the acquisition of cerebellar learning, by using optogenetics and animal behavioral tests [47].

Mitochondrial Calcium Uniporter (*Mcu*) complex regulates mitochondrial Ca^{2+} uptake, which ensures Ca^{2+} accumulation inside mitochondrial matrix due to increases in cytosolic Ca^{2+} and regulates cytosolic Ca^{2+} signaling, energy production and cell death [38-40]. In mammals, the uniporter complex (uniplex) contains four core components: the pore-forming *Mcu*, gatekeeper MICU1 and MICU2, and an auxiliary EMRE subunit essential for Ca^{2+} transport. Previous studies have suggested that *Mcu*-regulated calcium homeostasis is associated with oxidative stress and many neurological diseases [41-46]. In the present study, we have found the high level of *Mcu* expression dots on dendrites **(Fig. 3E)** of Purkinje cells. In view of this, it is reasonable to speculate it is due to *Mcu* which provides flexibility to the cerebellum in its role in producing appropriate behavioral responses to different adaptive stimuli.

At the same time, Ca^{2+} release is under the control of the Na^{+}/Ca^{2+} exchanger, encoded by the *Nclx* gene, and of a H^{+}/Ca^{2+} antiporter [48]. Our results have confirmed the expressions of *Nclx* on the Purkinje cells. Previously, Roome CJ et al. indicated that reverse-mode *Nclx* functioned as a new route for fast presynaptic Ca^{2+} entry at the cerebellar parallel fiber-to Purkinje neuron synapse, which verified the importance of the *Nclx* in the Purkine cells [49].

Our results illustrated that *Nclx* and *Mcu* were expressed in Purkinje cells, which have confirmed that *Mcu* and *Nclx* in the inner membrane contribute to the function of mitochondria and mitochondrial calcium homeostasis are important for Purkinje cells. Thus *Mcu* & *Nclx* would be the potential therapeutic targets in neurological diseases in the future.

4.3 *Ucp2* and *Ucp4*

Mitochondrial uncoupling proteins (UCPs), a subfamily of the mitochondrial transporter family, which is located in the inner mitochondrial membrane, dissipates the proton gradient between the intermembrane space and the mitochondrial matrix to uncouple electron transport from ATP synthesis [50]. Expression of mRNA for Ucp2, and *Ucp4* has been found at high levels in brain [50]. Ucp2, a protein located in the inner mitochondrial membrane, may regulate mitochondrial energy metabolism and ROS generation [51,52]. Coppola et al. and Andrews et al. showed that increased mitochondria number in neuronal perikarya is promoted by *Ucp2* in the arcuate nucleus [53,54]. *Ucp2* in VMH neurons changes mitochondria, such as increase in mitochondrial density and reduction in mitochondrial size, suggesting that the expression of *Ucp2* is related with mitochondrial fission regulated by *Drp1* [55]. Richard D et al. found that *Ucp2* mRNA expressed highly in the cerebellum by in situ hybridization studies [56]. *Ucp4*, another member of the mitochondrial transporter family, more widespread expressed in the brain and has the same functions [54]. Of our results, *Ucp2* showed lower expression than *Ucp4* in the Purkinje cell body, which consisted with previous studies. Lacking neuronal UCPs causes mitochondrial dysfunction (decreased ATP, increased oxidative stress and calcium dysregulation) and might influence plasticity and neurotransmission, all of which affect neurodegenerative pathologies [54]. From our previous results, *Ucp4* located at the cerebellum shows sensitivity to the stress and up-regulated [57]. Consequently, we hypothesized that *Ucp4* in Purkinje cells could serve as a preindicator of purkinje cell-related diseases. Once purkinje cells suffer damage, *Ucp4* shows corresponding changes, although there are no behavioral changes.

4.4 Limitation

Unfortunately, in our study, we have not performed the patch clamp study which could record the electrical characteristics of purkinje cells. So we did not know the special high frequency of spontaneous action potential of Purkinje cells has changed or not in the present Cre-LoxP transgenic mice. Moreover, although we have found the convergence of *Drp1*, *Ucp4* and *Mfn2* in Purkinje cells, the relative functions of these molecules on clinical diseases have not been investigated here. It is expected that we will provide definitive guidelines for purkinje cells related clinical diseases in the future.

Conclusion

When applied to the purkinje cells of the cerebellum, our approach yielded a number of insights. First, we verified the convergence of mitochondrial proteins *Drp1*/ *Mfn2*/ *Mcu*/ *Ucp4* on the purkinje cells in situ. Second, we generated GAD2-cre:ZsGreen-tdTomatofl/fl mice to allow resolving of purkinje cell-specific mitochondrial changes under multiple pathological conditions because of their high-resolution imaging

for purkinje cells, both by light microscopy and electron microscopy. Third, mitochondrial proteins topographical analysis of our cerebellar RNAscope resulted in clear predictions for differentially regulated mitochondrial dynamic mechanisms, which could be studied in the further research. Fourth, the lack of *Mfn1*/ *Nclx*/ *Ucp2* indicated the unique intracellular mitochondrial mechanisms in Purkinje cells related to the cell distinct morphology, firing pattern and synaptic plasticity.

Drp1 controls dendritic arborization and mitochondrial transpor in Purkinje cells [58]. Mitochondria of the PC in cerebellum become elongated and large sphere followed *Drp1* KO due to constrict fission [59] *Mfn2* is critical for dendrite growth, spinal formation, and cell survival in Purkinje cells, while *Mfn1* shows no significant effect from previous study [34]. Dysfunction of *Mcu* reduced the calcium influx into the cytosol of Purkinje cells , which rescued AFG3L2-induced ataxia [60]. *Nclx* functions as a new route for fast presynaptic Ca^{2+} entry at the cerebellar PF-PN (parallel fiber-to Purkinje neuron) synapse. From previous research, there were no studies performed on *Ucp2* or *Ucp4* in PC [49]. From our previous results, we hypothesized that *Ucp4* in Purkinje cells could serve as a preindicator of purkinje cell-related diseases.

Rocha A et al. and Chen H et al. reported that Mutations in *Mfn2* cause neurodegenerative Charcot-Marie-Tooth disease type 2A (CMT2A) [61,34]. Girard M et al. claimed that mitochondrial dysfunction and Purkinje cell loss in autosomal recessive spastic ataxia of Charlevoix-Saguenay (ARSACS) [62]. AFG3L2, a gene encodes a subunit of the mitochondrial m-AAA protease, previously famous as a quality control protein for misfolding inner mitochondrial membrane proteins and famous for regulatory functions through processing of specific substrates. And mutations in the AFG3L2 gene have been associated with spinocerebellar ataxia type 28 and spastic ataxia-neuropathy syndrome in humans [63,64]. These previous researches confirmed the importance of the mitochondria in cerebellum or Purkinje cells. Purkinje cells are the sole output of the computational circuitry of the cerebellar cortex and provide the signals required for motor planning, execution and coordination in their rate of firing and pattern of activity [65]. There is no doubt that the fate of PC is closely related to clinical diseases.

Our results showed that *Drp1*, *Mfn2* and *Ucp4* exhibited high convergence in cerebellar Purkinje cells. According to the previous research, a large amount of literature has shown that these molecules are very important for the maintenance of Purkinje cell health. The damage of these molecules will lead to the dysfunction of mitochondria, and then result in the damage of Purkinje cells, which is manifested as clinical diseases such as ARSACS [62], ataxia [63,64], neural degeneration [66] and so on. Considering the relativity between these molecules and purkinje cells disease, we speculated that the high convergence of these molecules in mitochondria may form a homeostasis chain for keeping the Purkinje cells fit, which we named as molecular homeostasis chain. And the molecule as a member of the chain interact, restrict or cooperate with each other in function. Once the expression of a molecule is abnormal and beyond the range of cell self-regulation, the molecular homeostasis chain will suffer a huge impact, causing irreversible damage to Purkinje cells, accompanied by clinical disease. Therefore, the high convergence of *Ucp4*, *Mfn2* and *Drp1* observed in our results are very important for the health maintenance of Purkinje cells and mitochondria. The abnormal expression of these molecules may provide reference value for clinical Purkinje cell related diseases. For the diseases that have occurred, regulating the expression of

these molecules and stabilizing the cell homeostasis chain may provide a new direction for the clinical treatment of Purkinje cell related diseases.

Abbreviations

Acronym	Full name
A	Axons
ACD	Advanced Cell Diagnostics
ANOVA	Analysis of variance
ATP	Adenosine-triphosphate
CB	Calbindin
D	Dendritic arbors
dapB	4-hydroxy-tetrahydrodipicolinate reductase
DAPI	2-(4-Amidinophenyl)-6-indolecarbamidine dihydrochloride
Drp1	Dynamin-related protein 1
DWF	Dendritic Weighted Formula
GABA	γ-aminobutyric acid
GAD	Glutamic acid decarboxylase
GCL	Granular layer
GFAP	Glial fibrillary acidic protein
IMM	Inner mitochondrial membrane
Mcu	Mitochondrial calcium uniporter
Mfn1	Mitofusion 1
Mfn2	Mitofusion 2
ML	Molecular layer
Nclx	Sodium/lithium/calcium exchanger
NeuN	Neuron specific nuclear protein
OMM	Outer mitochondrial membrane
PB	Phosphate buffer
PBS	Phosphate buffered saline
Pcp2	Purkinje cell protein 2
PCL	Purkinje cell layer
PCR	Polymerase chain reaction
PFA	Paraformaldehyde

PF-PN	parallel fiber-to Purkinje neuron
Polr2a	RNA polymerase II subunit A
PPIB	Peptidylprolyl isomerase B
ROS	Reactive oxygen species
SWF	Soma Weighted Formula
UBC	Ubiquitin C
Ucp2	Uncoupling protein 2
Ucp4	Uncoupling protein 4

Declarations

Funding This work was supported by the National Natural Science Foundation of China (81870415) from YL.Y., Xijing Hospital Boosting Plan (XJZT19Z29) from YL.Y., Military Medicine Upgrade Program of Air Force Military Medical University (2020SWAQ04) from YY.W., Health Services Project of Air Force Military Medical University (21WQ023) from YY.W., The project of science and technology to improve the combat effectiveness of school flight personnel (2019ZTC03) and Open Project of State Key Laboratory of Military Stomatology (2018KA01) of YY.W..

Competing interests The authors declare no competing interests.

Availability of data and materials The datasets used and analyzed during the current study are available from YY.W. on reasonable request.

Authors' contributions YY.W., YL.Y. and L.W designed the experiments. H.L. and TT.L.conducted the experiments. BL.G., KL.Z., SJ.L., XD.L. RQ.W. and JH.C. analyzed the data and participated in figures drawing. YY.W. and FF.W. wrote the manuscript. The authors read and approved the final manuscript.

Acknowledgments We thank all members of our lab for their helpful discussions and comments during the completion of this project.

Compliance with ethical standards

Ethical approval and consent to participate The experiments were performed according to the current laws of China.

References

1. Apps, R., & Garwicz, M. (2005). Anatomical and physiological foundations of cerebellar information processing. Nature reviews. Neuroscience, 6(4), 297– https://doi.org/10.1038/nrn1646
2. Louis ED and Faust PL. (2020). Essential tremor pathology: neurodegeneration and reorganization of neuronal connections. *Nat Rev Neurol*. 16, 69-83. https://doi.org/10.1038/s41582-019-0302-1
3. Pan MK, Li YS, Wong SB, Ni CL, Wang YM, Liu WC, et al (2020) Cerebellar oscillations driven by synaptic pruning deficits of cerebellar climbing fibers contribute to tremor pathophysiology. *Sci Transl Med.* 12(526), eaay1769. https://doi.org/10.1126/scitranslmed.aay1769
4. Kostadinov D, Beau M, Blanco-Pozo M, Häusser M. (2019). Predictive and reactive reward signals conveyed by climbing fiber inputs to cerebellar Purkinje cells. *Nat Neurosci.* 22, 950-962. https://doi.org/1038/s41593-019-0381-8.
5. Patron M, Sprenger HG, Langer T. (2018). m-AAA proteases, mitochondrial calcium homeostasis and neurodegeneration. *Cell Res*. 28, 296-306. https://doi.org/1038/cr.2018.17
6. Fecher C, Trovò L, Müller SA, Snaidero N, Wettmarshausen J, Heink S, et al. (2019). Cell-type-specific profiling of brain mitochondria reveals functional and molecular diversity. *Nat Neurosci.* 22, 1731-1742. https://doi.org/10.1038/s41593-019-0479-z
7. Cunnane SC, Trushina E, Morland C, Prigione A, Casadesus G, Andrews ZB, et al. (2020). Brain energy rescue: an emerging therapeutic concept for neurodegenerative disorders of ageing. *Nat Rev Drug Discov*. 19, 609-633. https://doi.org/1038/s41573-020-0072-x
8. Taniguchi H, He M, Wu P, Kim S, Paik R, Sugino K, et al. (2011). A resource of Cre driver lines for genetic targeting of GABAergic neurons in cerebral cortex. *Neuron* 71, 995-1013. https://doi.org/10.1016/j.neuron.2011.07.026
9. Fish KN, Rocco BR, DeDionisio AM, Dienel SJ, Sweet RA, Lewis DA. (2021). Altered Parvalbumin Basket Cell Terminals in the Cortical Visuospatial Working Memory Network in Schizophrenia. *Biol Psychiatry.* 90, 47-57. https://doi.org/10.1016/j.biopsych.2021.02.009
10. Muzumdar MD, Tasic B, Miyamichi K, Li L, Luo L. (2007). A global double-fluorescent Cre reporter mouse. *Genesis* 45, 593-605. https://doi.org/10.1002/dvg.20335
11. Huang J, Wang Y, Wang W, Wei Y, Li Y, Wu S. (2008). Preproenkephalin mRNA is expressed in a subpopulation of GABAergic neurons in the spinal dorsal horn of the GAD67-GFP knock-in mouse. Anat Rec (Hoboken). 291, 1334-1341. https://doi.org/10.1002/ar.20755

12. Wang F, Flanagan J, Su N, Wang LC, Bui S, Nielson A, et al. (2012). RNAscope: a novel in situ RNA analysis platform for formalin-fixed, paraffin-embedded tissues. *J Mol Diagn.* 14, 22-29. https://doi.org/10.1016/j.jmoldx.2011.08.002
13. Paxinos G and Franklin KBJ (1997) *The Mouse Brain in Stereotaxic Coordinates*, 2nd ed, Academic Press.
14. Fe Lanfranco M, Loane DJ, Mocchetti I, Burns MP, Villapol S. (2017). Combination of Fluorescent in situ Hybridization (FISH) and Immunofluorescence Imaging for Detection of Cytokine Expression in Microglia/Macrophage Cells. *Bio Protoc*. 7, e2608. https://doi.org/21769/BioProtoc.2608
15. Gebara E, Zanoletti O, Ghosal S, Grosse J, Schneider BL, Knott G, et al. (2021). Mitofusin-2 in the Nucleus Accumbens Regulates Anxiety and Depression-like Behaviors Through Mitochondrial and Neuronal Actions. *Biol Psychiatry*. 89, 1033-1044. https://doi.org/10.1016/j.biopsych.2020.12.003
16. Fagan, M., Scorr, L., Bernhardt, D., Hess, E. J., Perlmutter, J. S., Pardo, C. A., & Jinnah, H. A. (2021). Neuropathology of blepharospasm. Experimental neurology, 346, 113855. https://doi.org/10.1016/j.expneurol.2021.113855
17. Miwa, H., Kobayashi, K., Hirai, S., Yamada, M., Watanabe, M., Okado, H., & Yanagawa, Y. (2021). GAD67-mediated GABA Synthesis and Signaling Impinges on Directing Basket Cell Axonal Projections Toward Purkinje Cells in the Cerebellum. Cerebellum (London, England), 10.1007/s12311-021-01334-8. Advance online publication. https://doi.org/10.1007/s12311-021-01334-8
18. Singh-Bains MK, Linke V, Austria MDR, Tan AYS, Scotter EL, Mehrabi NF, et al. (2019). Altered microglia and neurovasculature in the Alzheimer's disease cerebellum. *Neurobiol Dis*. 132, 104589. https://doi.org/10.1016/j.nbd.2019.104589
19. Yawno T, Sutherland AE, Pham Y, Castillo-Melendez M, Jenkin G, Miller SL. (2019). Fetal Growth Restriction Alters Cerebellar Development in Fetal and Neonatal Sheep. *Front Physiol*. 10, 560. https://doi.org/10.3389/fphys.2019.00560
20. Levite M, Zelig D, Friedman A, Ilouz N, Eilam R, Bromberg Z, et al. (2020). Dual-Targeted Autoimmune Sword in Fatal Epilepsy: Patient's glutamate receptor AMPA GluR3B peptide autoimmune antibodies bind, induce Reactive Oxygen Species (ROS) in, and kill both human neural cells and T cells. *J Autoimmun*. 112, 102462. https://doi.org/10.1016/j.jaut.2020.102462
21. Janakiraman U, Dhanalakshmi C, Yu J, Moutal A, Boinon L, Fukunaga K, et al. (2020). The investigation of the T-type calcium channel enhancer SAK3 in an animal model of TAF1 intellectual disability syndrome. *Neurobiol Dis.* 143, 105006. https://doi.org/10.1016/j.nbd.2020.105006
22. Guan, J., Luo, Y., & Denker, B. M. (2005). Purkinje cell protein-2 (*Pcp2*) stimulates differentiation in PC12 cells by Gbetagamma-mediated activation of Ras and p38 MAPK. The Biochemical journal, 392(Pt 2), 389– https://doi.org/10.1042/BJ20042102
23. Berrebi, A. S., & Mugnaini, E. (1992). Characteristics of labeling of the cerebellar Purkinje neuron by L7 antiserum. Journal of chemical neuroanatomy, 5(3), 235– https://doi.org/10.1016/0891-0618(92)90048-u

24. Luo TT, Dai CQ, Wang JQ, Wang ZM, Yang Y, Zhang KL, et al. (2020). *Drp1* is widely, yet heterogeneously, distributed in the mouse central nervous system. *Mol Brain* 13, 90. https://doi.org/10.1186/s13041-020-00628-y
25. Chandra R, Engeln M, Schiefer C, Patton MH, Martin JA, Werner CT, et al. (2017). *Drp1* Mitochondrial Fission in D1 Neurons Mediates Behavioral and Cellular Plasticity during Early Cocaine Abstinence. *Neuron* 96, 1327-1341. https://doi.org/10.1016/j.neuron.2017.11.037
26. Bordt EA, Clerc P, Roelofs BA, Saladino AJ, Tretter L, Adam-Vizi V, et al.(2017). The Putative *Drp1* Inhibitor mdivi-1 Is a Reversible Mitochondrial Complex I Inhibitor that Modulates Reactive Oxygen Species. *Dev Cell* 40, 583-594. https://doi.org/10.1016/j.devcel.2017.02.020
27. Ishihara N, et al. (2009). Mitochondrial fission factor *Drp1* is essential for embryonic development and synapse formation in mice. *Nat Cell Biol*. 11, 958-966. https://doi.org/1038/ncb1907
28. Wakabayashi J, Zhang Z, Wakabayashi N, Tamura Y, Fukaya M, Kensler TW, et al. (2009). The dynamin-related GTPase *Drp1* is required for embryonic and brain development in mice. *J Cell Biol*. 186, 805-816. https://doi.org/10.1083/jcb.200903065
29. Kageyama Y, Hoshijima M, Seo K, Bedja D, Sysa-Shah P, Andrabi SA, et al. (2014). Parkin-independent mitophagy requires *Drp1* and maintains the integrity of mammalian heart and brain. *EMBO J*. 33, 2798-2813. https://doi.org/10.15252/embj.201488658
30. Frank S, Gaume B, Bergmann-Leitner ES, Leitner WW, Robert EG, Catez F, et al. (2001). The role of dynamin-related protein 1, a mediator of mitochondrial fission, in apoptosis. *Dev Cell*. 1, 515-525. https://doi.org/10.1016/s1534-5807(01)00055-7
31. Lackner LL and Nunnari J. (2010). Small molecule inhibitors of mitochondrial division: tools that translate basic biological research into medicine. *Chem Biol*. 17, 578-583. https://doi.org/10.1016/j.chembiol.2010.05.016
32. Grohm J, Kim SW, Mamrak U, Tobaben S, Cassidy-Stone A, Nunnari J, et al. (2012). Inhibition of *Drp1* provides neuroprotection in vitro and in vivo. *Cell Death Differ*. 19, 1446-1458. https://doi.org/1038/cdd.2012.18
33. Oettinghaus B, Licci M, Scorrano L, Frank S. (2012). Less than perfect divorces: dysregulated mitochondrial fission and neurodegeneration. *Acta Neuropathol*. 123, 189-203. https://doi.org/1007/s00401-011-0930-z
34. Chen H, McCaffery JM, Chan DC. (2007). Mitochondrial fusion protects against neurodegeneration in the cerebellum. *Cell* 130, 548-562. https://doi.org/10.1016/j.cell.2007.06.026
35. Züchner S, Mersiyanova IV, Muglia M, Bissar-Tadmouri N, Rochelle J, Dadali EL, et al. (2004). Mutations in the mitochondrial GTPase mitofusin 2 cause Charcot-Marie-Tooth neuropathy type 2A. *Nat Genet*. 36, 449-451. https://doi.org/1038/ng1341
36. Chung KW, Kim SB, Park KD, Choi KG, Lee JH, Eun HW, et al. (2006). Early onset severe and late-onset mild Charcot-Marie-Tooth disease with mitofusin 2 (*Mfn2*) mutations. *Brain* 129, 2103-2118. https://doi.org/10.1093/brain/awl174

37. Ishikawa K, Yamamoto S, Hattori S, Nishimura N, Tani H, Mito T, et al. (2019). Acquired Expression of Mutant Mitofusin 2 Causes Progressive Neurodegeneration and Abnormal Behavior. *J Neurosci*. 39, 1588-1604. https://doi.org/10.1523/JNEUROSCI.2139-18.2018
38. Rizzuto R, De Stefani D, Raffaello A, Mammucari C. (2012). Mitochondria as sensors and regulators of calcium signalling. *Nat Rev Mol Cell Biol*. 13, 566-578. https://doi.org/1038/nrm3412
39. Giorgi C, Marchi S, Pinton P. (2018). The machineries, regulation and cellular functions of mitochondrial calcium. *Nat Rev Mol Cell Biol*. 19, 713-730. https://doi.org/1038/s41580-018-0052-8
40. Fan M, Zhang J, Tsai CW, Orlando BJ, Rodriguez M, Xu Y, et al. (2020). Structure and mechanism of the mitochondrial Ca^{2+} uniporter holocomplex. *Nature* 582, 129-133. https://doi.org/1038/s41586-020-2309-6
41. Baughman JM, Perocchi F, Girgis HS, Plovanich M, Belcher-Timme CA, Sancak Y, et al. (2011). Integrative genomics identifies *Mcu* as an essential component of the mitochondrial calcium uniporter. *Nature* 476, 341-345. https://doi.org/1038/nature10234
42. De Stefani D, Patron M, Rizzuto R. et al. (2015). Structure and function of the mitochondrial calcium uniporter complex. *Biochim Biophys Acta*. 1853, 2006- https://doi.org/10.1016/j.bbamcr.2015.04.008
43. Peng TI and Jou MJ. (2010). Oxidative stress caused by mitochondrial calcium overload. *Ann N Y Acad Sci*. 1201, 183- https://doi.org/10.1111/j.1749-6632.2010.05634.x
44. Owens K, et al. (2013). Mitochondrial dysfunction and NAD(+) metabolism alterations in the pathophysiology of acute brain injury. *Transl Stroke Res.* 4, 618- https://doi.org/10.1007/s12975-013-0278-x
45. Di Lisa F and Bernardi P. (2009). A CaPful of mechanisms regulating the mitochondrial permeability transition. *J Mol Cell Cardiol*. 46, 775- https://doi.org/10.1016/j.yjmcc.2009.03.006
46. Zhang L, Wang H, Zhou X, Mao L, Ding K, Hu Z. (2019). Role of mitochondrial calcium uniporter-mediated Ca2+ and iron accumulation in traumatic brain injury. *J Cell Mol Med*. 23, 2995-3009. https://doi.org/1111/jcmm.14206
47. Bonnan, A., Rowan, M., Baker, C. A., Bolton, M. M., & Christie, J. M. (2021). Autonomous Purkinje cell activation instructs bidirectional motor learning through evoked dendritic calcium signaling. Nature communications, 12(1), 2153. https://doi.org/10.1038/s41467-021-22405-8
48. De Stefani D, Rizzuto R and Pozzan T. (2016). Enjoy the Trip: Calcium in Mitochondria Back and Forth. *Annu Rev Biochem.* 85, 161-192. https://doi.org/10.1146/annurev-biochem-060614-034216
49. Roome, C. J., Power, E. M., & Empson, R. M. (2013). Transient reversal of the sodium/calcium exchanger boosts presynaptic calcium and synaptic transmission at a cerebellar synapse. Journal of neurophysiology, 109(6), 1669– https://doi.org/10.1152/jn.00854.2012
50. Sherkhane, P., & Kapfhammer, J. P. (2017). Chronic pharmacological blockade of the Na+ /Ca2+ exchanger modulates the growth and development of the Purkinje cell dendritic arbor in mouse cerebellar slice cultures. The European journal of neuroscience, 46(5), 2108–2120. https://doi.org/10.1111/ejn.13649

51. Kim-Han, J. S., & Dugan, L. L. (2005). Mitochondrial uncoupling proteins in the central nervous system. Antioxidants & redox signaling, 7(9-10), 1173–1181. https://doi.org/10.1089/ars.2005.7.1173

52. Mattiasson, G., Shamloo, M., Gido, G., Mathi, K., Tomasevic, G., Yi, S., Warden, C. H., Castilho, R. F., Melcher, T., Gonzalez-Zulueta, M., Nikolich, K., & Wieloch, T. (2003). Uncoupling protein-2 prevents neuronal death and diminishes brain dysfunction after stroke and brain trauma. Nature medicine, 9(8), 1062–1068. https://doi.org/10.1038/nm903

53. Coppola, A., Liu, Z. W., Andrews, Z. B., Paradis, E., Roy, M. C., Friedman, J. M., Ricquier, D., Richard, D., Horvath, T. L., Gao, X. B., & Diano, S. (2007). A central thermogenic-like mechanism in feeding regulation: an interplay between arcuate nucleus T3 and Ucp2. Cell metabolism, 5(1), 21–33. https://doi.org/10.1016/j.cmet.2006.12.002

54. Andrews, Z. B., Liu, Z. W., Walllingford, N., Erion, D. M., Borok, E., Friedman, J. M., Tschöp, M. H., Shanabrough, M., Cline, G., Shulman, G. I., Coppola, A., Gao, X. B., Horvath, T. L., & Diano, S. (2008). *Ucp2* mediates ghrelin's action on NPY/AgRP neurons by lowering free radicals. Nature, 454(7206), 846–851. https://doi.org/10.1038/nature07181

55. Toda, C., Kim, J. D., Impellizzeri, D., Cuzzocrea, S., Liu, Z. W., & Diano, S. (2016). *Ucp2* Regulates Mitochondrial Fission and Ventromedial Nucleus Control of Glucose Responsiveness. Cell, 164(5), 872–883. https://doi.org/10.1016/j.cell.2016.02.010

56. Richard, D., Huang, Q., Sanchis, D., & Ricquier, D. (1999). Brain distribution of *Ucp2* mRNA: in situ hybridization histochemistry studies. International journal of obesity and related metabolic disorders : journal of the International Association for the Study of Obesity, 23 Suppl 6, S53–S55. https://doi.org/10.1038/sj.ijo.0800947

57. Wu, F. F., Zhang, K. L., Wang, Z. M., Yang, Y., Li, S. H., Wang, J. Q., Ma, J., Yang, Y. L., Zhang, H. F., & Wang, Y. Y. (2021). Benefit of a single simulated hypobaric hypoxia in healthy mice performance and analysis of mitochondria-related gene changes. Scientific reports, 11(1), 4494. https://doi.org/10.1038/s41598-020-80425-8

58. Fukumitsu, K., Hatsukano, T., Yoshimura, A., Heuser, J., Fujishima, K., & Kengaku, M. (2016). Mitochondrial fission protein *Drp1* regulates mitochondrial transport and dendritic arborization in cerebellar Purkinje cells. Molecular and cellular neurosciences, 71, 56–65. https://doi.org/10.1016/j.mcn.2015.12.006

59. Kageyama, Y., Zhang, Z., Roda, R., Fukaya, M., Wakabayashi, J., Wakabayashi, N., Kensler, T. W., Reddy, P. H., Iijima, M., & Sesaki, H. (2012). Mitochondrial division ensures the survival of postmitotic neurons by suppressing oxidative damage. The Journal of cell biology, 197(4), 535–551. https://doi.org/10.1083/jcb.201110034

60. Patron, M., Sprenger, H. G., & Langer, T. (2018). m-AAA proteases, mitochondrial calcium homeostasis and neurodegeneration. Cell research, 28(3), 296–306. https://doi.org/10.1038/cr.2018.17

61. Rocha, A. G., Franco, A., Krezel, A. M., Rumsey, J. M., Alberti, J. M., Knight, W. C., Biris, N., Zacharioudakis, E., Janetka, J. W., Baloh, R. H., Kitsis, R. N., Mochly-Rosen, D., Townsend, R. R.,

Gavathiotis, E., & Dorn, G. W., 2nd (2018). *Mfn2* agonists reverse mitochondrial defects in preclinical models of Charcot-Marie-Tooth disease type 2A. Science (New York, N.Y.), 360(6386), 336–341. https://doi.org/10.1126/science.aao1785

62. Girard, M., Larivière, R., Parfitt, D. A., Deane, E. C., Gaudet, R., Nossova, N., Blondeau, F., Prenosil, G., Vermeulen, E. G., Duchen, M. R., Richter, A., Shoubridge, E. A., Gehring, K., McKinney, R. A., Brais, B., Chapple, J. P., & McPherson, P. S. (2012). Mitochondrial dysfunction and Purkinje cell loss in autosomal recessive spastic ataxia of Charlevoix-Saguenay (ARSACS). Proceedings of the National Academy of Sciences of the United States of America, 109(5), 1661–1666. https://doi.org/10.1073/pnas.1113166109
63. Almajan, E. R., Richter, R., Paeger, L., Martinelli, P., Barth, E., Decker, T., Larsson, N. G., Kloppenburg, P., Langer, T., & Rugarli, E. I. (2012). AFG3L2 supports mitochondrial protein synthesis and Purkinje cell survival. The Journal of clinical investigation, 122(11), 4048–4058. https://doi.org/10.1172/JCI64604
64. Tunc, S., Dulovic-Mahlow, M., Baumann, H., Baaske, M. K., Jahn, M., Junker, J., Münchau, A., Brüggemann, N., & Lohmann, K. (2019). Spinocerebellar Ataxia Type 28-Phenotypic and Molecular Characterization of a Family with Heterozygous and Compound-Heterozygous Mutations in AFG3L2. Cerebellum (London, England), 18(4), 817–822. https://doi.org/10.1007/s12311-019-01036-2
65. Attwell, D., & Mehta, A. R. (2021). Anatomy embroiders function in Purkinje cells. The Lancet. Neurology, 20(10), 793. https://doi.org/10.1016/S1474-4422(21)00281-7
66. Richard, D., Rivest, R., Huang, Q., Bouillaud, F., Sanchis, D., Champigny, O., & Ricquier, D. (1998). Distribution of the uncoupling protein 2 mRNA in the mouse brain. The Journal of comparative neurology, 397(4), 549–560. https://doi.org/10.1002/(SICI)1096-9861(19980810)397:4<549::AID-CNE7>3.0.CO;2-1

Tables

Table 1. The primers sequences and program were used to identify specific genotype.

	Primers for mutant type	Primers for wild-type allele
Gad2-cre	CTTCTTCCGCATGGTCATCT	CTTCTTCCGCATGGTCATCT
	CACCCCACTGGTTTTGATTT	AAAGCAATAGCATCACAAATTTCA
ZsGreen-tdTomato$^{fl/fl}$	ATGCCCACCAAAGTCATCAGTGTAG	GGGCAGTCTGGTACTTCCAAGCT
	AGGCGGGCCATTTACCGTAAGTTA	ATATCCCCTTGTTCCCTTTCTGC
Gad2^{tdTomato}/non-Gad2^{ZsGreen}	CTTCTTCCGCATGGTCATCT	CTTCTTCCGCATGGTCATCT
	CACCCCACTGGTTTTGATTT	AAAGCAATAGCATCACAAATTTCA
	ATGCCCACCAAAGTCATCAGTGTAG	GGGCAGTCTGGTACTTCCAAGCT
	AGGCGGGCCATTTACCGTAAGTTA	ATATCCCCTTGTTCCCTTTCTGC

The PCR program used was as follows:

94°C for 3 min, then 35 cycles of 94°C for 30 s for denaturation, 62°C for 35 s for annealing, and 72°C 45 s for elongation.

Table 2. The antibodies were used to verify the purkinje cells in Gad2^{tdTomato}/non-Gad2^{ZsGreen} mice.

Antibody type	Antibody name	Mark for different cerebellar cells	Company	Product number	Dilution condition	Species
Primary antibody	**Anti-Calbindin**	**Purkinje cells**	Abcam	Ab75524	1: 500	Mouse
	Anti-NeuN	**Granule cells**	Abcam	ab177487	1: 500	Rabbit
	Anti-GFAP	**Astrocytes**	Cell Signaling	12389	1: 500	Rabbit
	Anti-Iba1	**Microglia**	Reagent	SKM6526	1: 500	Rabbit
Secondary antibody	**Dylight 649, Goat Anti-Rabbit IgG**		Abbkine	A23620	1: 500	Rabbit
	Dylight 649, Goat Anti-Mouse IgG		Abbkine	A23610	1: 500	Mouse
Nucleus dye	**DAPI**		Beyotime	C1005	1: 1000	

Table 3. The probes were used in RNAscope in situ hybridization.

Name	Mitochondrial localization	Function	Accession number	Target region	Dilution	TSA® Plus channel
Drp1	OMM	Mitochondrial fission	NM_152816.3	793-1845	1 : 1	1
Mfn1	OMM	Mitochondrial fusion	NM_024200.4	1059-2413	1 : 1	1
Mfn2	OMM	Mitochondrial fusion	NM_001285920.1	795-1230	1 : 50	3
Mcu	IMM	Mitochondrial calcium intruder	NM_001033259.4	148-1206	1 : 50	2
Nclx	IMM	Mitochondrial calcium extruder	NM_133221.2	429-1459	1 : 50	3
Ucp2	IMM	Mitochondrial uncoupling	NM_011671.5	2-1002	1 : 1	1
Ucp4	IMM	Mitochondrial uncoupling	NM_028711.4	457-1410	1 : 50	3
Pcp2		Purkinje cell marker	NM_001129804.1	2-302	1 : 50	2
Polr2a	Positive control		NM_009089.2	2802-3678	1 : 1	1
PPIB	Positive control		NM_011169.2	98-856	1 : 1	2
UBC	Positive control		NM_019639.4	34-860	1 : 1	3
DapB	Negative control		EF191515	414-862	1 : 1	1, 2, 3

Drp1, dynamin-related protein; ***Mcu***, mitochondrial calcium uniporter; ***Mfn1/2***, mitofusion 1/2; ***Nclx***, sodium/lithium/calcium exchanger; ***Pcp2***, Purkinje cell protein 2; **Ucp2/4**, uncoupling protein 2/4. **IMM** = Inner mitochondrial membrane; **OMM** = Outer mitochondrial membrane

Table 4. Semi-quantitative assessment to visualize the target mRNA expression level both the dendrite shafts and soma with of Purkinje cells by binning the percentage of constructs with a certain number of dots in one bin in cerebellum of Gad2-cre; ZsGreen-tdTomato$^{fl/fl}$ mice.

Mfn2 **mRNA**				
	% of Dendrite Shafts	Dendritic Weighted Formula	% of Soma	Soma Weighted Formula
Bin 0 (0 Dots / dendrite or soma)	12	0 * 4	0	0 * 0
Bin 1 (1-3 Dots / dendrite or soma)	52	+ 1 * 52	1	+ 1 * 1
Bin 2 (4-9 Dots / dendrite or soma)	4	+ 2 * 4	1	+ 2 * 1
Bin 3 (10-15 Dots / dendrite or soma)	0	+ 3 * 0	8	+ 3 * 8
Bin 4 (>15 Dots / dendrite or soma)	0	+ 4 * 0	28	+ 4 * 28
H-Score		**60**		**139**
Mcu **mRNA**				
	% of Dendrite Shafts	Dendritic Weighted Formula	% of Soma	Soma Weighted Formula
Bin 0 (0 Dots / dendrite or soma)	40	0 * 40	11	0 * 11
Bin 1 (1-3 Dots / dendrite or soma)	30	+ 1 * 30	18	+ 1 * 18
Bin 2 (4-9 Dots / dendrite or soma)	0	+ 2 * 0	2	+ 2 * 2
Bin 3 (10-15 Dots / dendrite or soma)	0	+ 3 * 0	0	+ 3 * 0
Bin 4 (>15 Dots / dendrite or soma)	0	+ 4 * 0	0	+ 4 * 0
H-Score		**70**		**22**
Nclx **mRNA**				
	% of Dendrite Shafts	Dendritic Weighted Formula	% of Soma	Soma Weighted Formula

Bin 0 (0 Dots / dendrite or soma)	55	0 * 55	10	0 * 10
Bin 1 (1-3 Dots / dendrite or soma)	4	+ 1 * 4	21	+ 1 * 21
Bin 2 (4-9 Dots / dendrite or soma)	1	+ 2 * 1	5	+ 2 * 5
Bin 3 (10-15 Dots / dendrite or soma)	0	+ 3 * 0	0	+ 3 * 0
Bin 4 (>15 Dots / dendrite or soma)	0	+ 4 * 0	0	+ 4 * 0
H-Score		**4**		**31**
***Ucp2* mRNA**				
	% of Dendrite Shafts	Dendritic Weighted Formula	% of Soma	Soma Weighted Formula
Bin 0 (0 Dots / dendrite or soma)	3	0 * 45	0	0 * 15
Bin 1 (1-3 Dots / dendrite or soma)	13	+ 1 * 15	0	+ 1 * 15
Bin 2 (4-9 Dots / dendrite or soma)	1	+ 2 * 0	0	+ 2 * 6
Bin 3 (10-15 Dots / dendrite or soma)	0	+ 3 * 0	14	+ 3 * 0
Bin 4 (>15 Dots / dendrite or soma)	0	+ 4 * 0	3	+ 4 * 0
H-Score		**15**		**27**
***Ucp4* mRNA**				
	% of Dendrite Shafts	Dendritic Weighted Formula	% of Soma	Soma Weighted Formula
Bin 0 (0 Dots / dendrite or soma)	3	0 * 3	0	0 * 0
Bin 1 (1-3 Dots / dendrite or soma)	14	+ 1 * 14	0	+ 1 * 4
Bin 2 (4-9 Dots / dendrite or	0	+ 2 * 0	0	+ 2 * 4

soma)				
Bin 3 (10-15 Dots / dendrite or soma)	0	+ 3 * 0	14	+ 3 * 25
Bin 4 (>15 Dots / dendrite or soma)	0	+ 4 * 0	3	+ 4 * 4
H-Score		**14**		**103**

The number of bins ranges from 0 - 4 according to the ACD scoring system. The overall H score can range from 0 - 400 and was calculated as methods described in the Methods. In our research, 3 mice were counted into our study, and each mouse was photographed with 3 images.

Figures

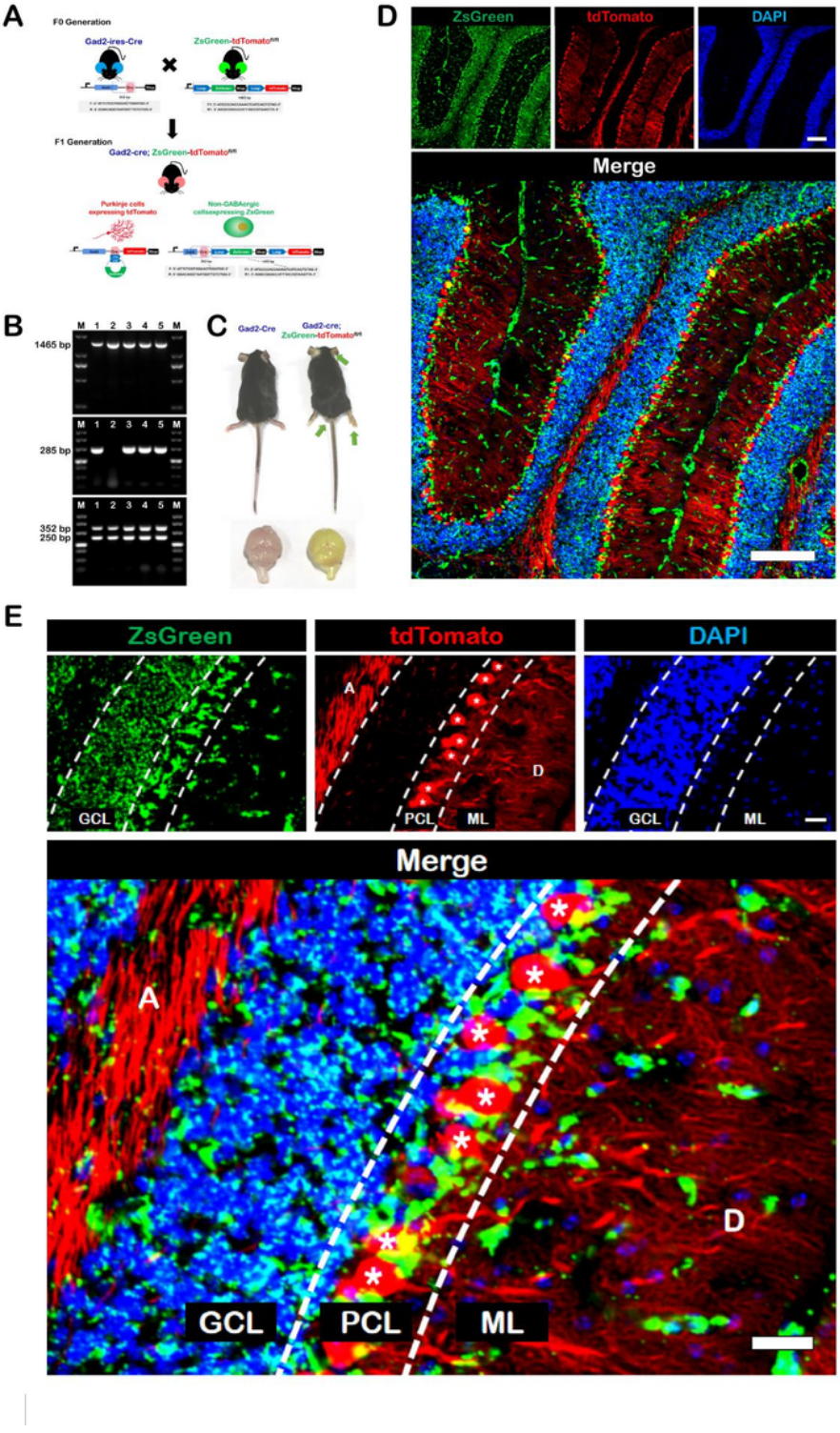

Figure 1

Purkinje cells specifically expressed tdTomato in GAD2-cre;ZsGreen-tdTomato$^{fl/fl}$ mice.

(A) Strategy to generate a conditional knock-in mice with specific fluorescence in GABAergic Purkinje cell by using cre-loxP system. The Gad2-ires-Cre mice inserted an ires and a Cre recombinase sequence at the 3' end of the Gad2 allele, so that all of GABAergic neurons contained Cre recombinase. In the ZsGreen-

tdTomato$^{fl/f}$ mice, ZsGreen and tdTomato were knocked in and the *loxP* sites were buried on both sides of ZsGreen. After crossing of these two mice, all GABAergic neurons in the newly generated transgenic Gad2-cre;ZsGreen-tdTomato$^{fl/fl}$ mice would transfer from expressing ZsGreen to expressing tdTomato due to Cre recombinase cutting loxP sites.

(B) Genotyping PCR results. The genotyping strategy used four sets of primers to produce four bands of 1465 bp (for ZsGreen-tdTomato with *loxP* site), 285 bp (for wild type site), 352 bp (Cre recombinase), and 250 bp (for for wild type site). So the mice numbered 1 and 3-5 in the picture with the four bands simultaneously, were Gad2-cre;ZsGreen-tdTomato$^{fl/fl}$ mice, who were used for the subsequent morphological observation.

(C) The pictures of bodies (up) and brains (down) of control Gad2-cre and Gad2-cre;ZsGreen-tdTomato$^{fl/fl}$ mice at P21. Average body weights were 10.2 ± 0.8 g (**Gad2-cre**; n = 10) and 10.2 ± 1.0 g (Gad2-cre;ZsGreen-tdTomato$^{fl/fl}$; n = 10), p = 0.80 (unpaired t test). Interestingly and apparently, Gad2-cre;ZsGreen-tdTomato$^{fl/fl}$ mice showed dazzling green light visible to the naked eye in external auricle skin (arrow), plantar skin (arrow), as well as perianal skin (arrow). It should be indicated that especially the brains of Gad2-cre;ZsGreen-tdTomato$^{fl/fl}$ mice showed green fluorescence, while the brains of control Gad2-cre mice showed normal pink, which made it very easy to distinguish the GABAergic knock-in mice.

(D) Confocal microscope image of cerebellar Purkinje cells expressing tdTomato in the cerebellum of Gad2-cre;ZsGreen-tdTomato$^{fl/fl}$ mice, together with non-GABAergic cells (expressing ZsGreen) and DAPI (blue) .

(E) The higher magnification of Figure D. It could be noted that the neuronal bodies of Purkinje cells with red fluorescence (asterisk marked in E) were aligned like dominos stacked throughout the PCL (Purkinje cell layer) like soldiers, also they had large dendritic arbors (D) like within the ML (molecular layer) and sent axons (A) like bright flame out off cerebellar cortex, therefore they left the dark area of GCL (granular cell layer) which were occupied by green non-GABAergic cells.

A, axons; **D,** dendritic arbors; **GCL,** granular cell layer; **ML,** molecular layer; **PCL,** Purkinje cell layer.

Scale bars: 200 μm **(D and E).**

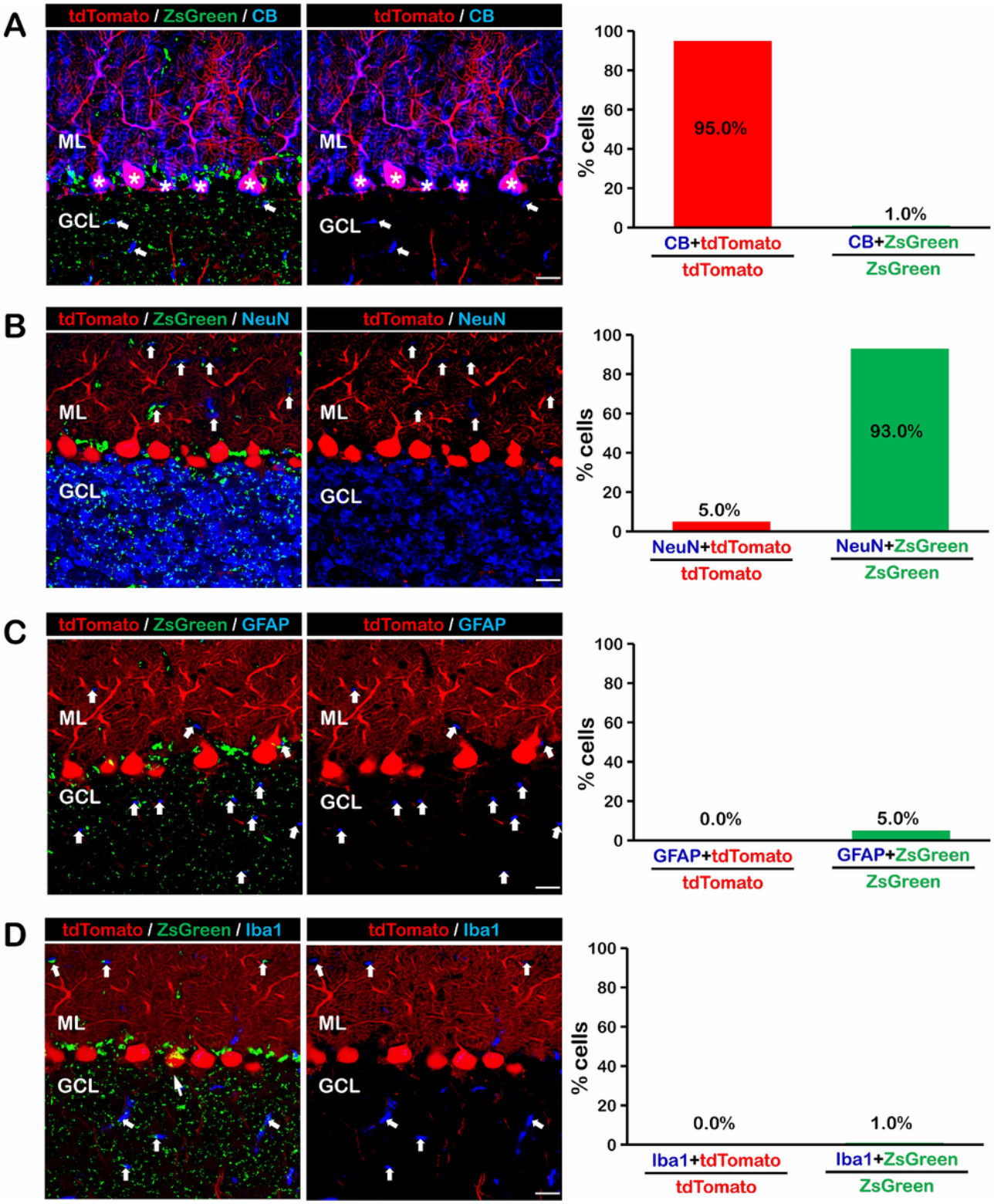

Figure 2

Double stainings verified Purkinje cells specifically expressing tdTomato fluorescence in GAD2-cre:ZsGreen-tdTomato$^{fl/fl}$ mice.

(A) Left: **tdTomato-positive cells (red)** were almost 100% colocalized with **calbinin (CB)**, **the marker of Purkinje cells (marked by asterisk)**; Right: Percentage of cells with co-expressing in CB with tdTomato- or

ZsGreen-positive cells in tdTomato- or ZsGreen-positive cells. Some arrows indicated that few **CB-positive structures** also scattered within GCL which consisted 1.0% cololization of CB and ZsGreen.

(B) Left: little **tdTomato-positive cells (red)** were colocalized with **NeuN, the marker of granular cells**; Right: Percentage of cells with co-expressing in NeuN with tdTomato- or ZsGreen-positive cells in tdTomato- or ZsGreen-positive cells. The arrows indicated that some **NeuN-positive structures** appeared in ML, but they did not colocalize with tdTomato fluorescence.

(C) Left: none of **tdTomato-positive cells (red)** were colocalized with **GFAP, the marker of astrocytes**; Right: Percentage of cells with co-expressing in GFAP with tdTomato- or ZsGreen-positive cells in tdTomato- or ZsGreen-positive cells. The arrows indicated that some **astrocytes** appeared in both ML and GCL, but they did not colocalized with tdTomato fluorescence.

(D) Left: none of **tdTomato-positive cells (red)** were colocalized with **Iba1, the marker of microglia**; Right: Percentage of cells with co-expressing in Iba1 with tdTomato- or ZsGreen-positive cells in tdTomato- or ZsGreen-positive cells. The arrows indicated that some **microglia** appeared in both ML and GCL, but they did not colocalized with tdTomato fluorescence.

CB, Calbinin**; GCL,** granular cell layer; **GFAP,** Glial fibrillary acidic protein; **ML,** molecular layer; **NeuN,** Neuron specific nuclear protein;

Scale bars: 20 μm.

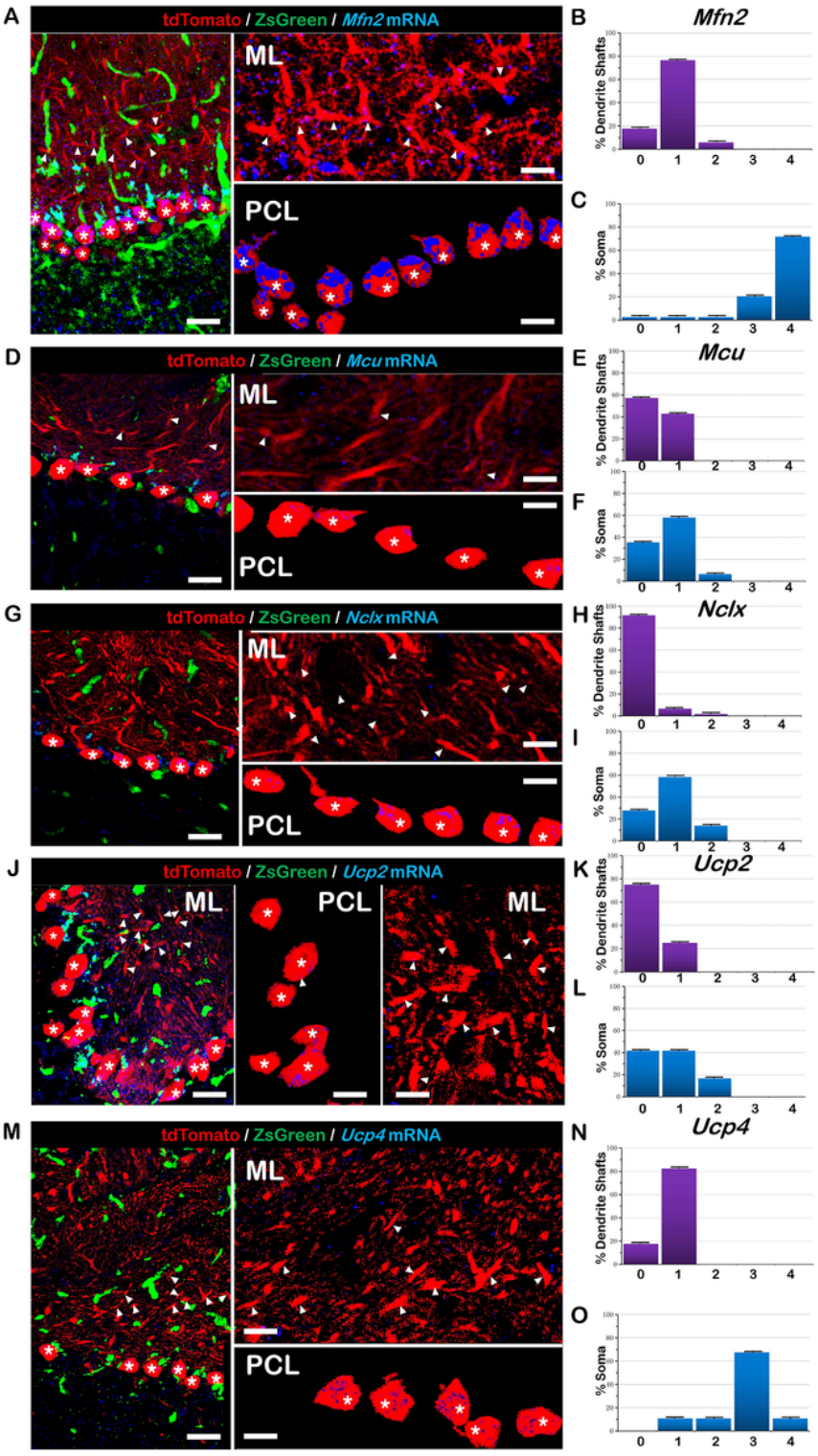

Figure 3

Identification of mRNAs of mitochondrial fusion, calcium transporter and uncoupling proteins (blue) in Purkinje cells (red) in the cerebellar cortex of GAD2-cre:ZsGreen-tdTomato$^{fl/fl}$ mice with RNAscope probes for *Mfn2*, *Mcu*, *Nclx*, *Ucp2* and *Ucp4* using the RNAscope. Green cells were non-GABAergic cells.

Representative RNAscope images showing the expression of **five types mRNAs (blue)** for *Mfn2* **(A)**, *Mcu* **(D)**, *Nclx* **(G)**, *Ucp2* **(J)** and *Ucp4* **(M)** in Purkinje cells (red) were in left picture, whose higher magnification images were shown in the relative right panels. Small tdTomato fluorescence spots can be seen around Purkinje cell, which might be other GABAergic neurons like the basket cells or Golgi cells.

In the right pictures, the expressions of mRNAs in dendrites were above marked by triangles within molecular layer (ML), while the expressions of mRNAs in soma were below marked by asterisk within Purkinje cell layer (PCL).

The graph above showed that ACD quantification of mRNAS for *Mfn2* **(B)**, *Mcu* **(E)**, *Nclx* **(H)**, *Ucp2* **(K)** and *Ucp4* **(N)** in dendrite shafts.

The graph below showed that ACD quantification of mRNAS for *Mfn2* **(C)**, *Mcu* **(F)**, *Nclx* **(I)**, *Ucp2* **(L)** and *Ucp4* **(O)** in soma.

ACD, Advanced Cell Diagnostics; **GAD,** Glutamic acid decarboxylase; ***Mcu*,** Mitochondrial calcium uniporter; ***Mfn2*,** Mitofusion 2; **ML,** Molecular layer; ***Nclx*,** Sodium/lithium/calcium exchanger; **PCL,** Purkinje cell layer; **Ucp2,** Uncoupling protein 2; ***Ucp4*,** Uncoupling protein 4.

Scale bars: 20 μm of the left panel **(in A, D, G, J and M)** and 10 μm of the right panel pictures **(in A, D, G, J and M)**.

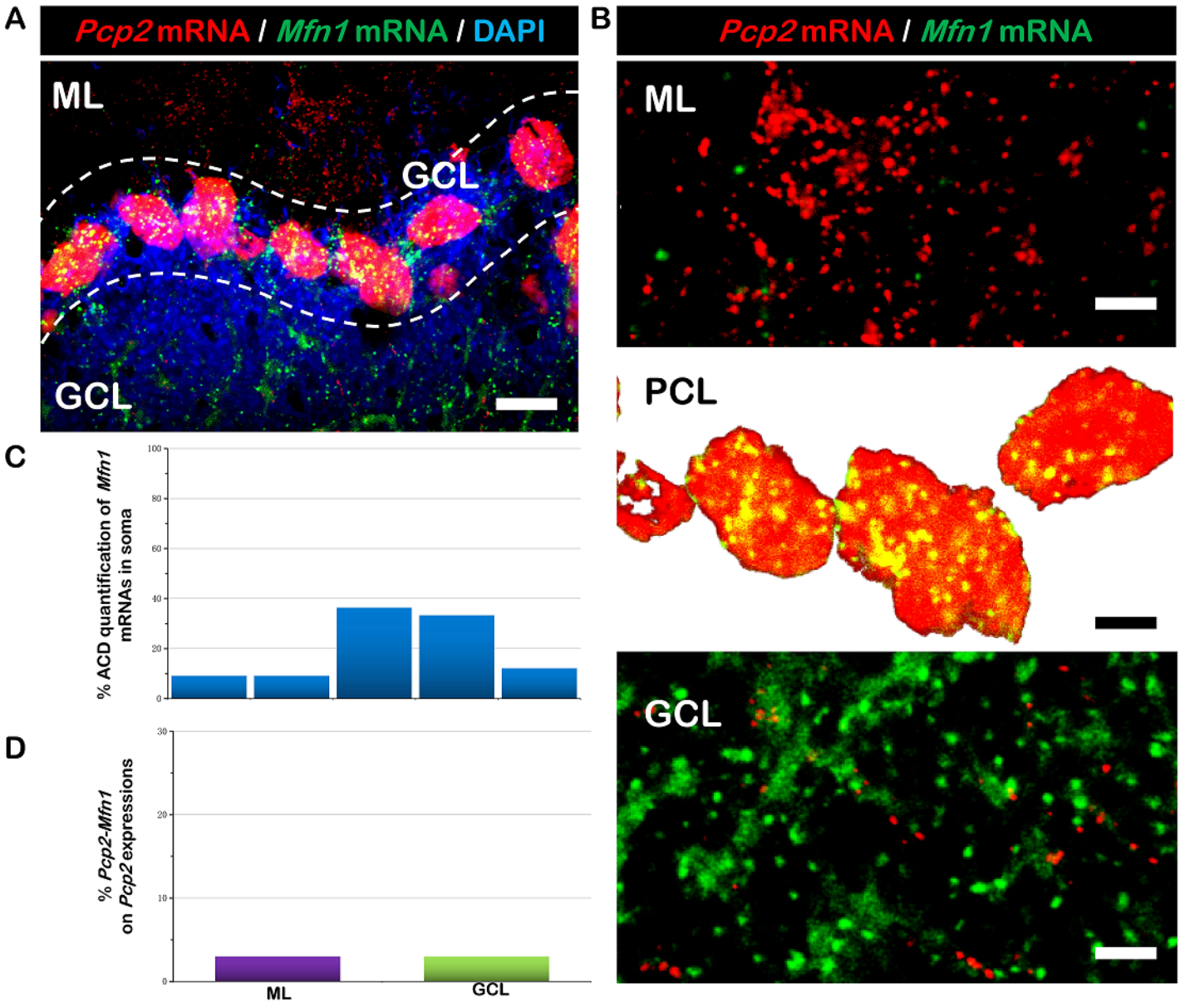

Figure 4

Detection of *Mfn1* (green) and *Pcp2* (red) in cerebellar cortex of C57BL/6 mice with the RNAscope Multiplex Fluoescent assay.

(A) Representative RNAscope images showing the expression of ***Mfn1* mRNA (green)** in **Purkinje cells (red)** which were distinguished by the red fluorescence with the mRNA probe of Purkinje cell protein-2 (*Pcp2*) gene. Three layers of molecular layer (ML), Purkinje cell layer (PCL) and granular cell layer (GCL) are outlined with **DAPI (blue)**.

(B) Higher magnification images of ***Mfn1* (green)** and ***Pcp2* (red)** RNAscopes in three layers of ML, PCL and GCL. Within the PCL, many yellow dots could be found in the soma of Purkinje cells (red). However, within both the ML and the GCL, few yellow dots could be found in the dendrites or axons of Purkinje cells, respectively.

(C) The graph showed that ACD quantification of mRNAS for *Mfn1* in soma.

(D) The graph showed % double *Pcp2-Mfn1* staining on *Pcp2*-positive expressions in ML and GCL.

GCL, granular cell layer; ***Pcp2,*** Purkinje cell protein 2; ***Mfn1,*** Mitofusion 1; **ML,** molecular layer; **PCL,** Purkinje cell layer.

Scale bars: 20 μm **(A and middle image of B)**; 10 μm **(up and down images in B**).

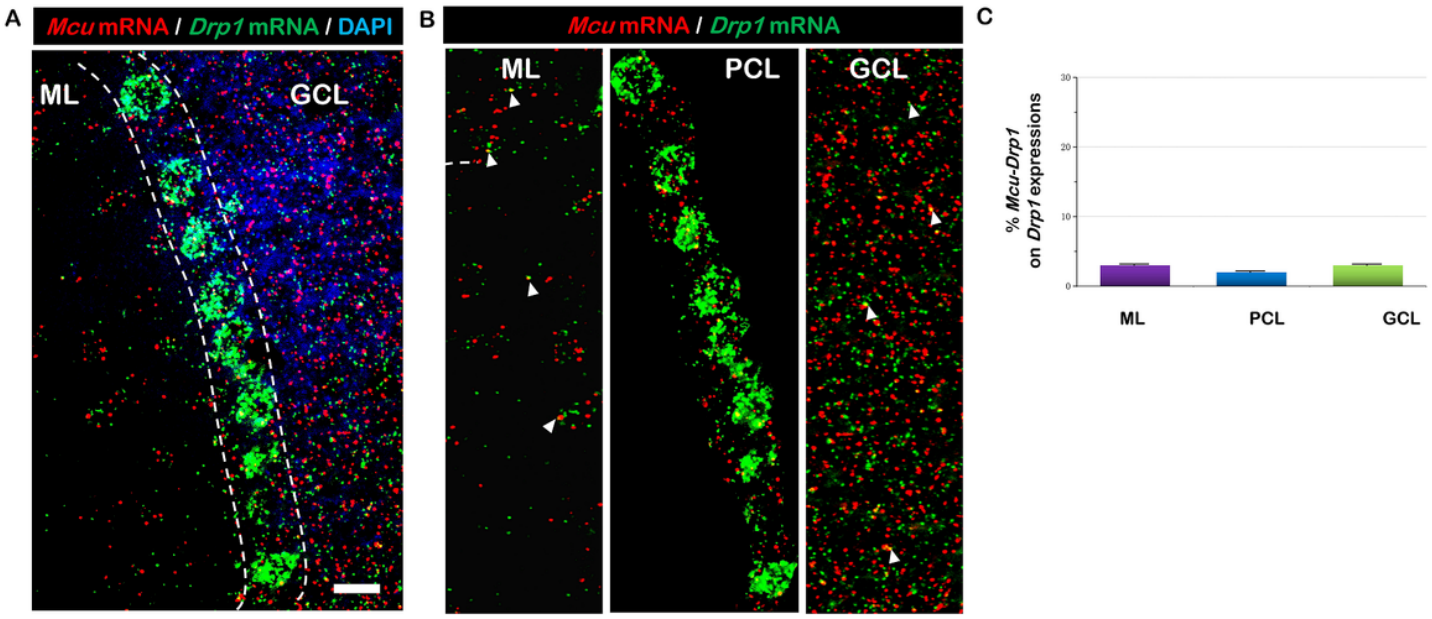

Figure 5

Detection of *Drp1* (green) and *Mcu* (red) in cerebellar cortex of C57BL/6 mice with the RNAscope Multiplex Fluoescent assay.

(A) Representative RNAscope images showing the expression of ***Mcu* mRNA (red)** in **Purkinje cells (green)** which were distinguished by the green fluorescence with the mRNA probe of *Drp1* gene. Three layers of molecular layer (ML), Purkinje cell layer (PCL) and granular cell layer (GCL) are outlined with DAPI (blue).

(B) Higher magnification images of ***Mcu* (red)** and ***Drp1* (green)** RNAscopes in three layers of ML, PCL and GCL. Within the PCL, green dots of *Drp1* could outline the soma of Purkinje cells. We found that very few red *Mcu* dots could be co-localizaed with green *Drp1* dots (indicated by white triangles).

(C) The graph showed % double *Drp1-Mcu* staining on *Drp1*-positive expressions in ML, PCL and GCL.

Drp1, Dynamin-related protein 1; **GCL,** granular cell layer; ***Mcu,*** Mitochondrial calcium uniporter; **ML,** molecular layer; **PCL,** Purkinje cell layer.

Scale bars: 20 μm **(A and B)**.

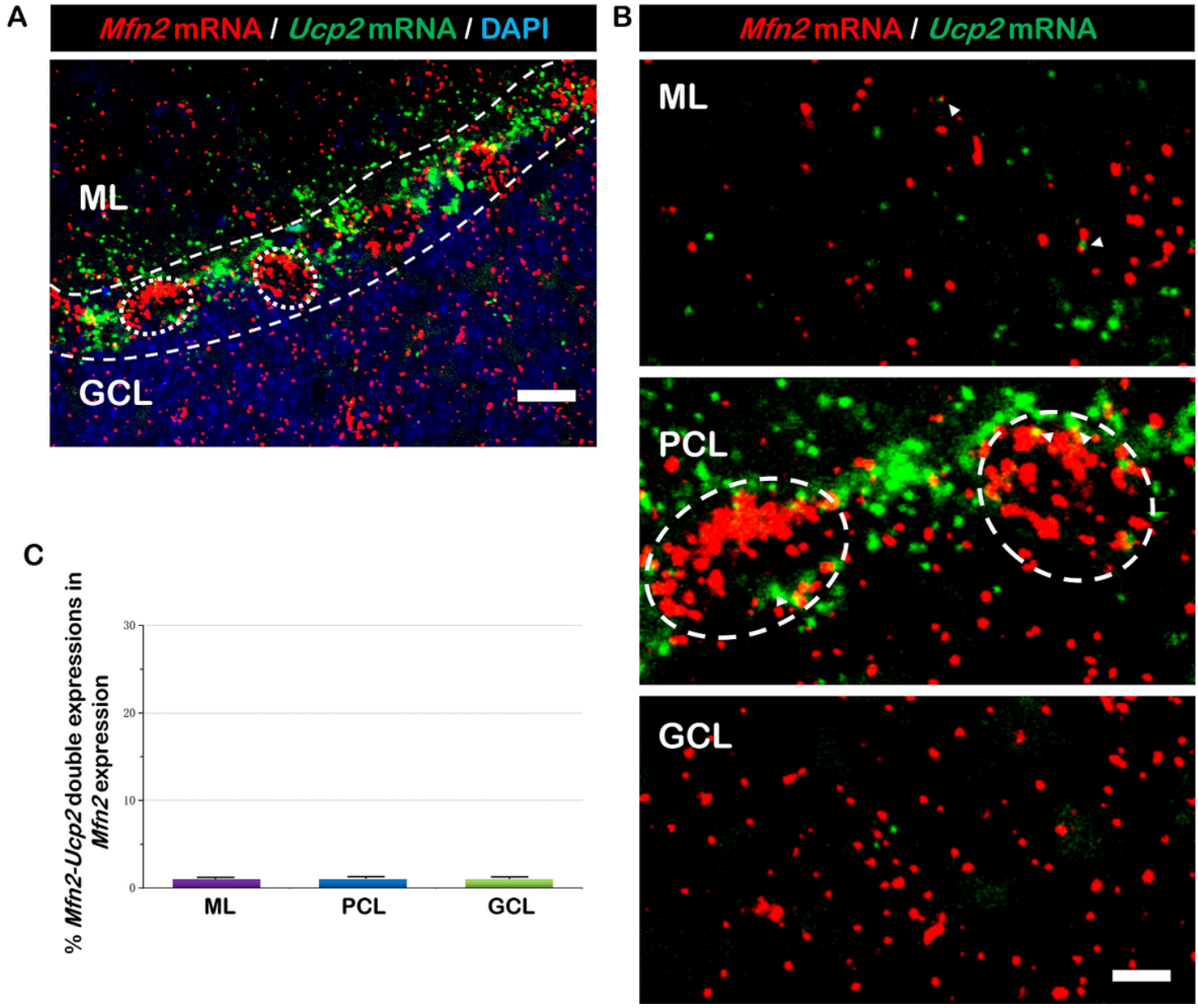

Figure 6

Detection of *Ucp2* (green) and *Mfn2* (red) in cerebellar cortex of C57BL/6 mice with the RNAscope Multiplex Fluoescent assay.

(A) Representative RNAscope images showing the expression of ***Ucp2* mRNA (green)** in **Purkinje cells (red)** which were distinguished by the red fluorescence with the mRNA probe of *Mfn2* gene (circlered by white dotted line). Three layers of molecular layer (ML), Purkinje cell layer (PCL) and granular cell layer (GCL) are outlined with DAPI (blue).

(B) Higher magnification images of ***Ucp2* (green)** and ***Mfn2* (red)** RNAscopes in three layers of ML, PCL and GCL. Within the PCL, red dots of *Mfn2* could outline the soma of Purkinje cells (white dotted circled).

We found that very few green *Ucp2* dots could be co-localizaed with red *Mfn2* dots (indicated by white triangles).

(C) The graph showed % double *Mfn2-Ucp2* staining on *Mfn2*-positive expressions in ML, PCL and GCL.

GCL, granular cell layer; ***Mfn2*,** Mitofusion 2; **ML,** molecular layer; **PCL,** Purkinje cell layer; **Ucp2,** Uncoupling protein 2.

Scale bars: 20 μm **(A)** and 10 μm **(B)**.

Supplementary Files

This is a list of supplementary files associated with this preprint. Click to download.

- SupplementaryFig1.tif
- SupplementaryFig2.tif
- Supplementary.docx
- video1redandblue.wmv
- video2greenandblue.wmv
- video3greenredandblue.wmv
- Graphicalabstract.tif